CHEMICAL REVIEWS

Volume 103, Number 10

Cathode Ray Tube Phosphors

Lyuji Ozawa

Consultant, L. L. Technology, Hopewell Junction, New York 12533

Minoru Itoh*

Department of Electrical and Electronic Engineering, Faculty of Engineering, Shinshu University, 4-17-1 Wakasato, Nagano 380-8553, Japan

Received January 7, 2003

Contents

1. Introduction 3835
2. Penetration of Primary Electrons into Crystals 3837
3. Excitation Mechanisms of Luminescence Centers in Phosphor Crystals 3842
4. Formation of Luminescence Centers in Phosphor Crystals 3843
   4.1. Donor–Acceptor Pair Recombination Centers 3843
      4.1.1. Band Model of ZnS 3843
      4.1.2. Luminescence Spectra of ZnS Phosphors 3844
      4.1.3. Decay Curves 3845
   4.2. Rare-Earth Recombination Centers 3845
      4.2.1. Luminescence Spectra of Y_2O_3 Phosphors 3846
      4.2.2. Luminescence Spectra of Other Oxide Phosphors 3848
      4.2.3. Decay Curves 3849
5. Optimized Energy Conversion Efficiencies of CRT Phosphors 3850
6. Appropriate Number of Photons Emitted from Phosphor Pixels in CRTs in Illuminated Rooms 3851
7. Advantage of CRTs as Display Devices 3851
8. Screenable Phosphor Powders on Faceplates of Color CRTs 3852
9. Conclusion 3854
10. References 3855

1. Introduction

If natural and synthesized crystals contain a small amount of impurities of transition elements (<1 mol %), they usually emit characteristic and sometimes brilliant luminescence under irradiation of invisible energetic particles such as ultraviolet photons, electrons, X-rays, and ion beams. These luminescent crystals are called phosphors (or luminescent materials), and the impurities are called activators (or luminescence centers). Because phosphors emit luminescence in the visible spectral region, they are good transducers (or detectors) in the study of invisible energetic particles in solids, in a vacuum, and in air. The luminescence stimulated by irradiation with an electron beam is named cathodoluminescence (CL). This article describes the characteristic properties of CL emitted from phosphor screens.

What follows is a brief review of CL studies. The phenomenon of CL has been known since the 19th century. In the early 19th century, many scientists studied some characteristic behaviors of free electrons, involving the interaction with magnetic and electrostatic fields in a vacuum. In their studies they used a cathode ray tube (CRT), in which electrons were subtracted from the pool of a plasma chamber (electrons and ions) into vacuum, and then were detected by the image illustrated on a phosphor screen placed in the CRT. This was possible because the phosphor screen emits visible CL. Almost all scientists of those days, however, gave attention to CL only as a good detector of electrons. Later, CL came to be used for detection of X-ray, ultraviolet light, and radiation from radioactive materials.

The studies of free electrons in a vacuum have achieved two important goals that have greatly influenced modern science and modern lives. One is the innovation of electronic devices that can amplify electric signals to some magnitude, and the other is the improvement of phosphor screens. The electronic

* Corresponding author. Tel.: +81-26-269-5261. Fax: +81-26-269-5220. E-mail: itohlab@gipwc.shinshu-u.ac.jp.

10.1021/cr0203490 CCC: $44.00
Published on Web 09/12/2003

Lyuji Ozawa has been involved in research on luminescent materials for more than 50 years, from basic research to applications and from screening of color and monochrome phosphor powders on substrates in CRTs to evaluation of image quality on phosphor screens. His current interest is the image quality on phosphor screens, such as flickerless, smearless, and high-contrast images like as printed images on sheets of paper. He is the author of three books, a coauthor of one, and the author of many journal papers.

Minoru Itoh received his doctorate degree in physics from Kyoto University in 1975 for studies concerning host-sensitized luminescence in alkali halides. He was a JSPS Fellow prior to taking a position at Shinshu University, where he is now a professor in the Department of Electrical and Electronic Engineering. His current research interests include luminescence properties of tungstates, lead halides, and oxides as scintillating materials, optical properties of phosphorescent crystals, photoinduced movement of impurity ions in alkali halides, investigation of new scintillating materials under core-level excitation, exploitation of nanometer-sized ultraviolet laser utilizing Auger-free luminescence, development of new experimental methods combining laser and synchrotron radiation, femtosecond relaxation phenomena induced by inner-shell excitation with high harmonics of high-power lasers, and theoretical studies of electronic structures of low-symmetry materials by quantum cluster calculation.

devices are now constructed by highly integrated electronic circuits on a tiny chip of solids, with good understanding of the behaviors of electrons and holes in solids (i.e., solid-state physics). Typical application fields of phosphor screens in modern lives are imaging screens in CRTs (transducers of electron beam in a vacuum), fluorescent lamps (converters of ultraviolet light to visible light), and X-ray imaging screens (converters of X-rays to visible light).

The CRT was invented by K. F. Braun in 1897, by using an oxide cathode as an electron source. These tubes are widely used in television sets and monitors of computers or oscilloscopes, after remarkable improvements based on an understanding of electron optics and electronics in a vacuum. However, CL mechanisms in phosphor crystals (solids) are not well understood, even though the brightness of the phosphor screen in CRTs has been greatly enhanced by the exploitation of phosphors with high quality. The quality of phosphors has been improved significantly over the past 50 years by experimental (and empirical) works, mainly purification of phosphor materials. The Leverentz (RCA Labs) and Kröger (Philips Labs) groups studied CL from phosphor screens extensively and systematically. They published excellent books summarizing their experimental works.[1,2] However, the mechanisms involved in the emission of CL remain still unresolved. The difficulty in studying CL is in the lack of knowledge of the fundamentals on the excitation mechanisms of luminescence centers in crystals (solids), e.g., (a) penetration of primary electrons into crystal, (b) excitation of luminescence centers by incident electrons, (c) formation of luminescence centers, and (d) energy conversion of penetrated electrons to CL. These problems are deeply related to the combination of two important factors: photon emission from luminescence centers and migration of free electrons in solids.

After clarification of the above-mentioned problems in this article, we will calculate the appropriate number of photons emitted from phosphor pixels in CRTs. The images on phosphor screens in CRTs are of practical importance. The light images we watch on CRTs are illustrated by means of the irradiation of a rapidly scanning high-energy electron beam, which is sharply focused into a point of less than 1 mm in diameter on the screen. Although one perceives uniformly emitted phosphor screens thanks to the effect of afterglow of the human eyes, the images are really illustrated as CL light spots (pixels) sequentially emitted on an entire phosphor screen. To study CL from a phosphor screen in a CRT, we have to investigate generation of instantaneous CL in phosphor pixels, rather than time- and space-averaged CL from the phosphor screen itself. The resolution of images is predominantly determined by the diameter of electron beams on a screen.[3] The brightness of scanning light spots depends on the energy density of electron beams dumped on phosphor pixels during the irradiation period. The qualities of the images on phosphor screens, such as whitening of the color and smearing and fading of the contrast, are highly correlated with the optical properties of the phosphor screens.

In this review, we will discuss (1) the penetration of primary electrons into solids, (2) the formation of luminescence centers, (3) energy conversion efficiencies of CRT phosphors, including excitation mechanisms of luminescence centers, and (4) the appropriate number of photons from phosphor pixels for display devices in illuminated rooms, on the basis of available data in the literature. These four points are essential for us to watch light images on CRTs comfortably. In addition, it is stressed that the CRTs have many advantages over other existing display devices. Further improvements of phosphor screens emitting CL will be performed by resolving a fair number of problems, such as (a) phosphor powders,

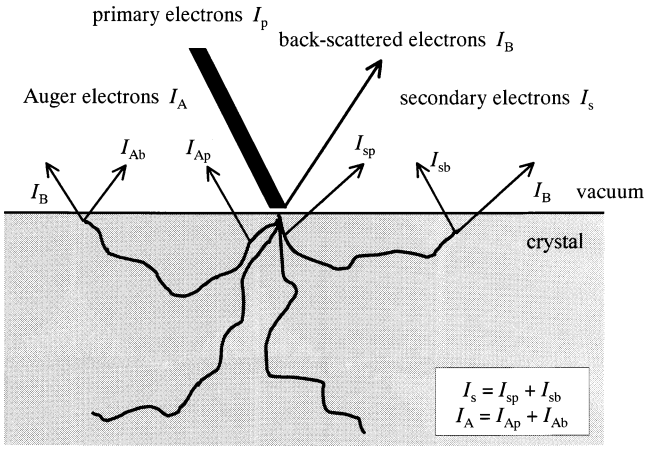

Figure 1. Schematic diagram of the production of secondary electrons, Auger electrons, and backscattered electrons. They are created by the irradiation of primary electrons.

(b) poly(vinyl alcohol) (PVA) phosphor slurry, (c) addition of surfactants, (d) drying of wet PVA phosphor screens, (e) photolithography on dried PVA phosphor screens, and so on. These important problems associated with CRTs will also be discussed in this review.

2. Penetration of Primary Electrons into Crystals

When a crystal is irradiated by an electron beam, a large part of the incident electrons penetrate into the crystal, and the residuals are ejected from the crystal surface, i.e., backscattered primary electrons due to the elastic scattering with the ions arranged in the surface layers of the crystal.[4,5] The penetrating electrons lose energy as a result of inelastic collisions with the lattice ions along the electron trajectories, generating X-rays, Auger electrons, secondary electrons, electron−hole pairs, and phonons. Figure 1 illustrates schematically the production of these secondary electrons. Advanced technology of surface physics and chemistry (analyzing the secondary electrons collected in front of the crystal) will provide us fruitful information on the generation of the secondary electrons in the crystals.

We will first discuss the secondary electrons ejected from phosphor crystals into a vacuum. Figure 2 shows a general energy spectrum of secondary electrons detected in front of the crystal surface. The spectrum consists of true secondary electrons, Auger electrons, characteristic loss electrons, and backscattered primary electrons. All of these electrons are now used as a powerful tool for better understanding of the surface physics and chemistry. The analysis of the backscattered primary electrons, i.e., low-energy electron diffraction (LEED) and high-energy electron diffraction (HEED), provides us detailed information on the structure of the crystal surface.

Due to the elastic and inelastic collisions with the lattice ions along the electron trajectory, the penetrating electrons generate Auger electrons and secondary electrons of energy smaller than that of the primary electrons. These secondary electrons can further generate other secondary electrons with smaller energies. This is an example of the cascade process of energy depletion. Assuming that the

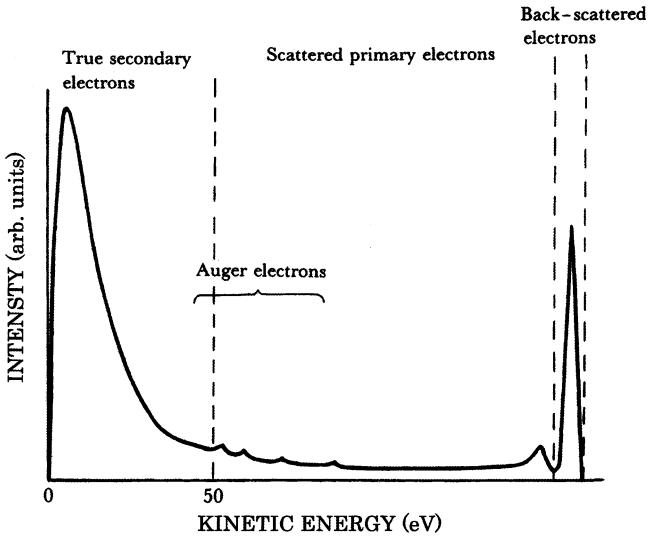

Figure 2. General energy spectrum of secondary electrons detected in front of the surface of a crystal.

internally generated secondary electrons form an electron-gas plasma, the lattice ions may be excited by plasma oscillations, i.e., by electron−plasmon interaction. Quinn has calculated the mean free path of plasma electrons for various energies.[6] His result is presented in Figure 3. The mean free path of the

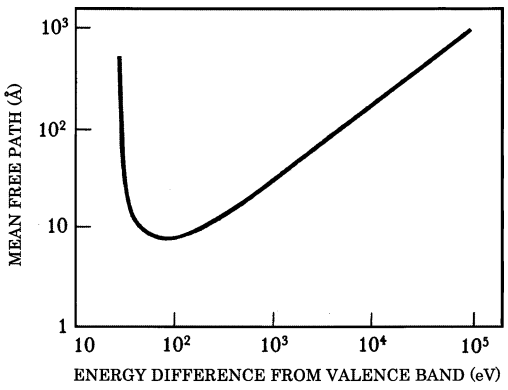

Figure 3. Mean free path of electrons to produce plasmons, as a function of the energy difference from the valence band.

plasma electrons in the energy range between 30 and 1000 V is about 10 Å. Hence, only the secondary electrons generated in the surface volume smaller than 10 Å in depth can escape from the crystal surface. On the other hand, Auger electrons are characterized by the elements in the surface volume, so the elements existing in a few atomic layers (about 10 Å in depth) can be identified from the Auger electron spectra.

A large part of the detected secondary electrons are widely distributed at energies below 50 eV, with a peak appearing at around a few eV. This part of the secondary electron spectra is not so dependent on the energy of incident electrons. These electrons are called true secondary electrons and are used in the scanning electron microscope. According to Amelio's model,[7] true secondary electrons are produced by the electron−plasmon interaction in the surface volume. His calculated and experimental curves for Cu metal and Si semiconductor are shown in Figure 4. The

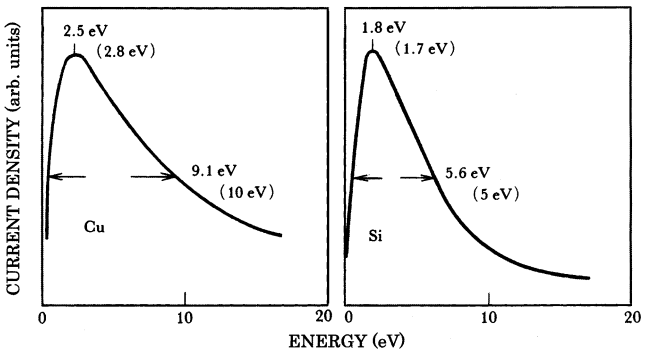

Figure 4. Theoretical prediction of the electron distribution of secondary electrons emitted from Cu and Si. Experimental values are indicated in parentheses.

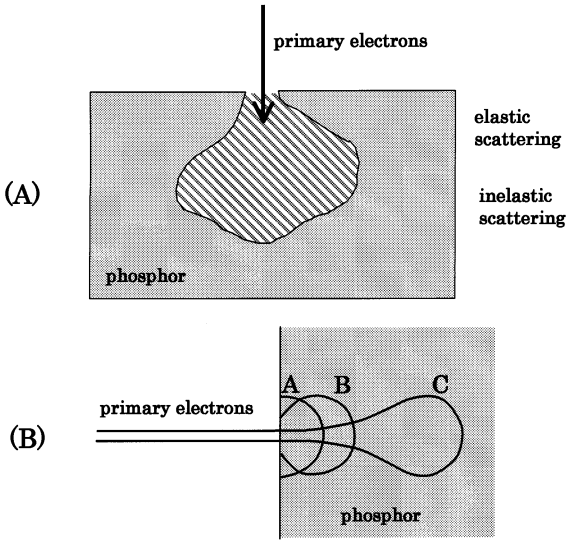

Figure 5. (A) Simulated scatting profile of primary electrons and (B) observed luminescence area in a phosphor. In (B), the energy of the primary electron beam is increased in the order of A, B, and C.

calculated values are in good agreement with the experimental results. These results not only verify the mechanisms of generation of true secondary electrons, but also support the presence of plasma electrons in the crystals.

Let us now discuss the secondary electrons generated in a crystal by the penetrating electrons. The penetrating electrons elastically and inelastically collide with the lattice ions and change their directions randomly at each collision event, losing energy through the production of secondary electrons. If Lewis's multiple scattering model (<10 kV)[8] or the single scattering model (>10 kV) is applied to the incident electrons, one can simulate the electron trajectories in a crystal using a Monte Carlo technique.[9−12] Figure 5A shows an example of the trajectories of incident electrons calculated by the single scattering model.[12] The luminescent area in a phosphor observed by Ehrenberg and Franks[13] is represented in Figure 5B, where the energy of primary electron beam is increased in order of A, B, and C.

Assuming that the internally generated secondary electrons also produce an electron plasma, the energy loss distribution and the penetration depth of incident electrons may, as a first-order approximation, be given by the profile of the electron trajectories of

Table 1. Observed and Calculated Values ΔE of the Energy Depletion in Various Compounds

		ΔE (eV)		
compd	Z^a	obsd	calcd	ref
ZnS	4	17	17	15
PbS	5	15	16	15
SbS_3	5.6	19	18	15
MoS_2	6	21	23	16
PbTe	5	15	14	15
PbSe	5	15	15	15
BeO	4	29	29	16
MgO	4	25	25	16
Li_2CO_3	4	24	24	16
$Ca(OH)_2$	3.2	22	21	16
MoO_3	6	25	24	16
SiO_2	5.3	25	25	16
Al_2O_3	4.8	25	27	16
TeO_2	6	23	23	16
SnO_2	4	18	26	15
KBr	4	20	13	16
KCl	4	13	14	15
NaCl	4	16	16	15

[a] Average number of valence electrons per atom that take part in plasma oscillation.

incident electrons. Figure 6 shows the calculated energy loss distribution and penetration depth of incident electrons in Al, Cu, and Au for various primary electron energies, e.g., 15 and 30 kV.[12] These profiles seem to be true for other crystals, too. The profile in phosphor crystals has been confirmed qualitatively from the observation of CL[13] and electron-sensitive films.[14] The electron trajectories may be clarified from both theoretical and experimental points of view. The assumption of the presence of plasmons could be supported by the data of the energy loss in crystals. Table 1 represents theoretical and experimental values of the energy loss in various compounds.[15,16] The theoretical calculation is based on the plasmon model. The theoretical values are in good agreement with the experimental ones. From Table 1, it may be concluded that the lattice ions in the bulk are excited by plasmons. If activator ions are excited only by plasmons, then all CL data must be explained by the plasmon model in the volume where the incident electrons have penetrated (smaller than the mean free path 10 Å). This volume V_d is defined by the energy of incident electrons, and the plasma electrons are distributed at random in V_d. Such a scenario, however, is not the case for CL (for example, see curve C in Figure 5B).

The plasma electrons also produce electron−hole pairs in the final stage of the energy loss process in crystals. These electron−hole pairs can move through the crystal out of the created volume, and some of them radiatively recombine at luminescence centers. The volume V_e is determined from the product of the cross section and the migration distance of electron−hole pairs. The volume V_e is always greater than V_d ($V_e > V_d$). Therefore, luminescence centers are excited by both plasmons (direct excitation) and mobile electrons and holes (indirect excitation), giving rise to the same characteristic activator luminescence. To get a good understanding of energy-transfer processes in the phosphor crystals, we have to know what type of mechanism is dominant for the excitation of

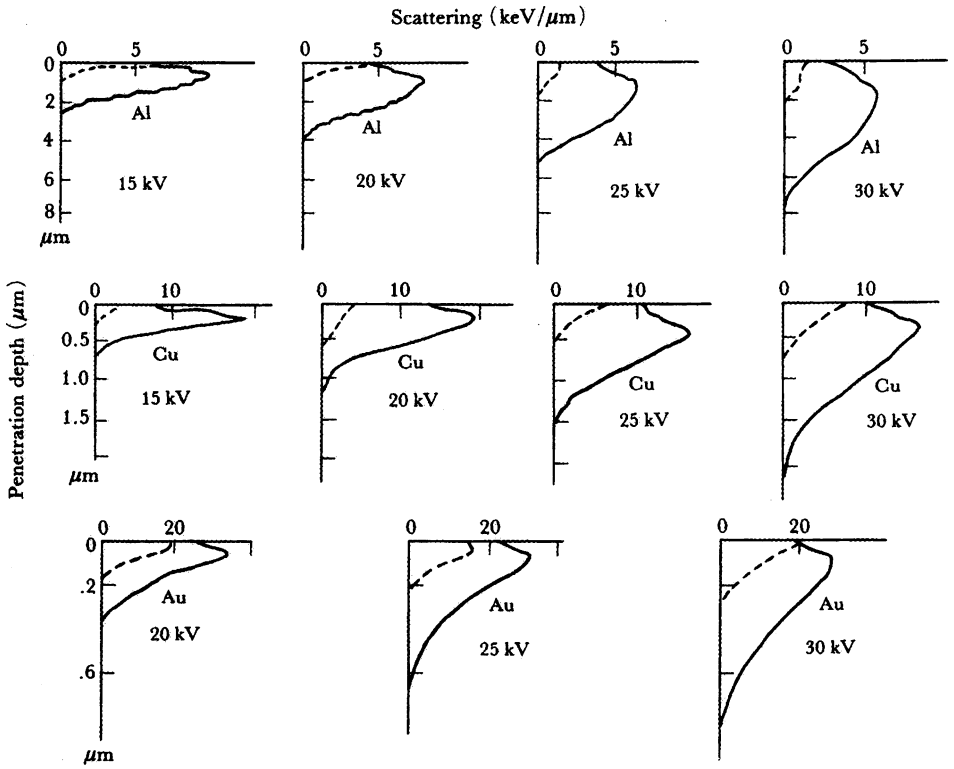

Figure 6. Energy loss curves of secondary electrons for various primary electron energies in Al, Cu, and Au at normal incidence: total energy loss (solid curve) and backscattering (dashed curve). Reprinted with permission from ref 37. Copyright 1990 Kodansha.

activator ions. However, we cannot distinguish among the excitation mechanisms from the luminescence spectrum alone, even though quite different excitation mechanisms are involved. It has been found that the concentration dependence curve of activator luminescence provides a useful tool in determining the type of excitations.[17] This will be described later.

In the above discussion, we assumed that the incident electrons always penetrate into a crystal. This is true only for conductive crystals. For insulators, the crystals are instantly charged negatively under electron beam irradiation. Late-arriving electrons interact with the negative electric field generated by the charged crystal and cannot reach the crystal surface. The process becomes more complicated when the surface-dead layer is considered. Both of the above effects must be clarified before going on to discuss the excitation of activator ions.

Semiconducting and insulating crystals, both being good host materials for phosphors, are covered with a layer. It is often called the surface-recombination (SR) layer for mobile electrons and holes.[18] Determination of the depth of the SR layer is a major subject of interest in the study of solid-state surface physics and chemistry. There is, however, no direct method to determine it. One method employed presently involves measuring the amount of free carriers[19] and/or the luminescence intensity[20] under the irradiation of electron beams as a function of the accelerating voltage. For a given crystal, the penetration depth of the incident electrons depends on the energy E of the electron beam.[21] This energy is determined by the anode potential V_p (i.e., $E = eV_p$, where e is the electron charge). If the crystal contains activator ions acting as radiative recombination centers for mobile electron−hole pairs, the activator luminescence provides us with an internal detector for studying the penetration of incident electrons into the crystal.[17] That is to say, the analysis of the time-averaged luminescence intensity $\langle I \rangle$ from activators as a function of the penetration depth of incident electrons (corresponding to V_p) will yield information about the depth of the SR layer.

It is assumed that, when the penetration depth of incident electrons is less than the depth of the SR layer, the electron beam irradiation results in no luminescence or faint luminescence due to the direct excitation of activator ions by the incident electrons. When the incident electrons penetrate through the SR layer, the penetrating electrons produce electron−hole pairs in the crystal volume (crystal bulk) deeper than the SR layer, resulting in much more intense activator luminescence due to the pair recombination.[17] Using this hypothesis, many authors have studied the voltage dependence of $\langle I \rangle$ in various phosphors.

The studies on the voltage dependence of $\langle I \rangle$ were conducted for phosphor screens in a demountable cathode ray picture tube configuration. The phosphor crystals forming the screen lie on the faceplate (substrate), which is usually an insulating (or conducting) glass and transparent for luminescence viewing. The curves A in Figure 7 show typical examples of the voltage dependence curves obtained with this configuration: linear voltage dependence of $\langle I \rangle$ is seen in the range around and above 3 kV, and faint luminescence is detected between 1 and 3 kV.[20−23] The crossing point of the linear dependence

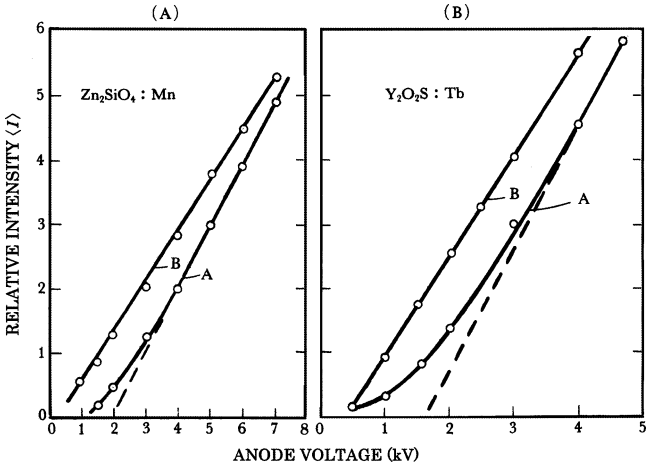

Figure 7. Voltage dependence curves of CL for two different screens of Zn_2SiO_4:Mn (A) and Y_2O_2S:Tb (B) phosphors. Curves A represent the results obtained for the screen prepared by sedimentation method using potassium silicate binder, and curves B represent the results obtained for the screen without binder.

(broken line) with the abscissa (about 2 kV) is called the "dead voltage".

The dead voltage was reported as being independent of the type of phosphors,[21−23] the degree of chemical etching of crystals, and the concentration of binders. This suggests that many investigators have measured improper voltage dependence curves in the range below 3 kV, even though the dead voltage in the high-voltage range above 2 kV changes with the thickness (>1000 Å) of the nonluminescent layer coating on the crystals.[21−27] The inorganic binder (e.g., silicate) used in the screening process, which adheres to the surface of the phosphor crystals, may influence the voltage dependence curve below 3 kV. To prove this, the curves ⟨*I*⟩ of commercial Zn_2SiO_4:Mn (screening weight density being 3 mg/cm^2) on a conductive glass plate were studied in two ways:[28] (i) sedimentation of phosphor particles on the plate using potassium silicate plus barium nitrate and (ii) sedimentation in deionized water without binder.

The measurements were carried out in a demountable tube under constant current density (10 μA/cm^2) by adjusting the spot size of the electron beam on a screen.[28] For the screen prepared with silicate binder, the result obtained is shown by curve A in Figure 7, which is similar to the curves reported by other groups,[25,27] although the screen was prepared with a different concentration of silicate binder. On the other hand, curve B of a screen prepared without binder is quite different from curve A; in the almost entire voltage range where luminescence is detected, ⟨*I*⟩ is linear with V_p, and the curve shifts considerably to the low-voltage side. The extrapolated line intersects at about 300 V. The curve moves to the high-voltage side with increasing thickness of the screen prepared without binder.

The experimental results described above lead to the conclusion that the thin phosphor screen on a conductive substrate must be prepared without binder, in order to study the voltage dependence curve of CL for the evaluation of SR layer. However, this is not always the case. For instance, the curves obtained on commercial ZnS:Cu (or Ag) phosphor, a typical CL phosphor, are the same as curve A, even if a thin phosphor screen on a conductive glass is prepared without binder. A study conducted using a scanning electron microscope showed that the surface of ZnS crystals is contaminated with submicrometer-size particles of insulators such as SiO_2.[29] The foreign insulators on ZnS crystals may have a predominant influence on the voltage dependence curve obtained in the range below 3 kV. The ZnS phosphor crystals without SiO_2 insulators also exhibit curve A. The surface of the produced ZnS crystals is covered with a thin layer of $Zn(OH)_2$ as a result of hydration.

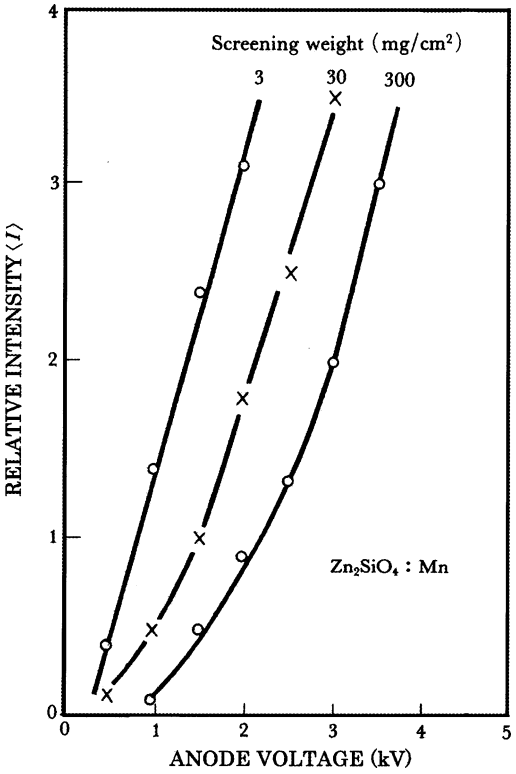

Figure 8. Voltage dependence curves of CL from the screen with different thickness in Zn_2SiO_4:Mn phosphors.

It has been experimentally shown[28] that the voltage dependence curve of CL significantly moves to the low-voltage side of curve A in Figure 7, if the measurements are made with a thin screen. In this experiment, thin screens were prepared on the conductive substrates with the phosphor crystals having no affixed foreign insulators on the surfaces. The threshold (dead) voltage of the curves varies with the thickness of the phosphor screen. This is seen from Figure 8.

We shall first consider the voltage dependence curve obtained with thin phosphor screens, which are prepared with and without binder (including the affixed foreign insulators on the crystal surface). Then, the threshold voltage dependence on the screen thickness will be discussed.

From the experimental results above, it is concluded that removing foreign insulators from the crystal surface is essential to determine the voltage dependence curve of phosphors in the range below 3 kV. Since the phosphor crystal itself (e.g., Zn_2SiO_4)

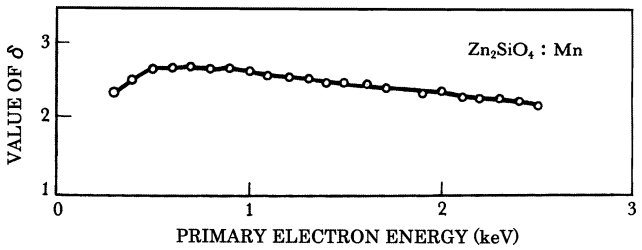

Figure 9. Plot of observed δ value against primary electron energy in Zn_2SiO_4:Mn phosphors.

is also a high insulator (electrical resistivity greater than 10^{10} Ω·cm), a question arises as to why the phosphor crystals give rise to curve B instead of curve A in Figure 7. This interesting question is explained by introducing a model based on surface-bound electrons (SBEs).

Cole and Cohen[30] showed theoretically the existence of SBEs outside an insulator, in a liquid, and in a solid. The secondary electrons generated in the surface volume, the depth of which is, e.g., less than 10 Å, are ejected from the crystal, leaving positive holes in the crystal. It has been reported that a penetrating electron with an accelerating voltage smaller than 3 kV collides a few times with the lattice ions, and each collision produces one secondary electron which can escape from the crystal.[31] This means that the ratio δ of the true secondary electrons to the entered electrons should be greater than 1. In fact, the reported δ values of various phosphors lie between 1.5 and 3,[32] irrespective of the primary electron energy (see Figure 9). As a result of more electrons being ejected from the crystal ($\delta > 1$) than entering ones, the crystal holds positive charges (holes) in the surface volume on the irradiation side. The positive electric field produced by holes will extend outside the crystal (in a vacuum) and attracts true secondary electrons. If the true secondary electrons having insufficient energy do not re-enter the crystal, the electrons are bound with the holes in the surface volume (i.e., SBEs). Eventually, a negatively charged electron cloud (space charges) is formed in front of the insulator after the incident electrons have entered the crystal. Figure 10 shows schematic pictures of SBEs.

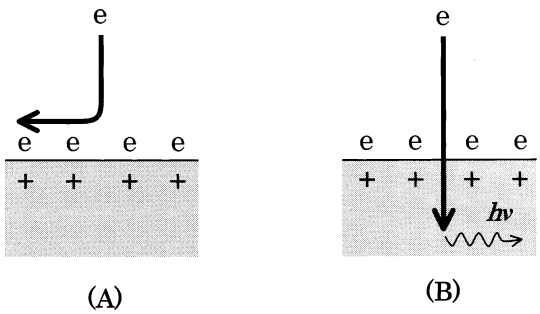

Figure 10. Schematic pictures of the interaction of incident electrons with surface-bound electrons (SBEs) formed in front of a crystal: (A) low-energy electron beam and (B) high-energy electron beam.

Since foreign insulators are uniformly distributed on the surface of phosphor crystals, the negative field produced by SBEs on the foreign insulators effectively shields the phosphor crystal. The negative shield thus prevents low-energy electrons from reaching the phosphor crystals; consequently, no or faint luminescence would be observed after a very short time, during which the first incident electrons have penetrated into the foreign insulators (see Figure 10A). Electrons having enough energy to penetrate through the shield can reach and enter the phosphor crystals, subsequently producing CL (see Figure 10B). This results in a constant threshold voltage (e.g., 2 kV) for the penetration. If this is so, the voltage dependence curve of phosphors is concealed in the characteristics of SBEs in the range below 3 kV. Therefore, the independence of the threshold (dead) voltage on the type of phosphors, the etching of crystals, and the concentration of binders would be explained by the concealment of SBEs on the foreign insulators.

With regard to the phosphor crystal having no foreign insulators on its surface, the SBEs lose the attracting partners and are liberated from the surface of the insulators when the holes in the surface volume are eliminated. By assuming that the crystal contains radiative (and/or nonradiative) recombination centers, the holes in the surface volume are partially (or totally) eliminated through the recombination with electrons at the centers if the crystal is conductive. Since efficient CL phosphors are photoconductive materials (i.e., conductive during irradiation of electron beam on the crystal) and always contain a large number of radiative recombination centers (e.g., $10^{-3}-10^{-2}$ mole fraction),[33] they can generate brilliant CL. If the threshold voltage is correlated with the effects of SBEs, it should be lowered from 2 kV, according to the equilibrium of the generation and elimination of holes in the surface volume. Curve B in Figure 7 is obtained on the screen of phosphors that have no affixed foreign insulators on the surface.

The threshold voltage progressively increases from 300 V with the increase in screen thickness and approaches 2 kV. This may be explained as follows. Sommer and Tanner[34] demonstrated experimentally the anisotropic mobility of SBEs. The mobility in the direction parallel to the crystal surface is remarkably low (a factor of 4−5) compared with that in the perpendicular direction. Brown and Grimes[35] confirmed the existence of the two-dimensional state (mobility) of SBEs outside liquid helium using the cyclotron resonance. Their results suggest that the SBEs can be removed from the surface of crystals by applying an external electric field, and the removal is easier in the parallel (horizontal) direction than in the perpendicular (vertical) direction.

The phosphor screen is built up of a number of randomly oriented tiny crystals of about 10 μm in size. Some of their faces are placed horizontally (or vertically), and others are inclined on the substrate. Therefore, the removal of SBEs is probably affected by the potential distribution over the particles arranged on the top layer of the screen,[36] which is more sensitive to the screen thickness, the screen construction, and other configurations. The electric field created by SBEs on the phosphor screens is estimated

to be 1×10^7 V/cm.[36]

Fortunately, many CRTs are operated between 10 and 30 kV, so that the electric field generated is 2×10^7 V/cm ($= 20 \times 10^3$ V/10 μm) at the top of the phosphor screen.[36] The SBE effects are thus relatively small. It can be safely assumed that in ordinary CL studies, the incident electron beam penetrates into the crystals and generates secondary electrons and electron−hole pairs. They can excite activator ions to emit CL. In the next section, we shall discuss the excitation mechanisms of activator ions (luminescence centers) in phosphor crystals by incident electrons.

3. Excitation Mechanisms of Luminescence Centers in Phosphor Crystals

Phosphor screens are constructed by arranging phosphor particles in layers. Since the penetration depth of incident electrons into phosphor particles is short (less than 1 μm[12]) as compared with the particle sizes (a few micrometers), generation of CL is restricted to the inside of phosphor particles arranged in the first layer of a screen on the electron gun side. Therefore, the excitation mechanisms of luminescence centers can be studied for phosphor particles with phosphor screens instead of single crystals. Possible excitation mechanisms of luminescence centers in phosphor particles are summarized as follows:

(a) direct collision of incident electrons with luminescence centers (direct excitation),

(b) resonance of high-velocity electrons with luminescence centers (plasmon excitation),

(c) charge transfer between associated activator and host lattice (charge-transfer excitation), and

(d) recombination of mobile electron−hole pairs at luminescence centers (indirect excitation through mobile carriers).

The characteristic CL arises from the electronic transitions in the luminescence center excited by one or a combination of the above-mentioned mechanisms. It is therefore impossible to identify the excitation mechanisms by measuring the CL spectrum. We must use other means for identification of excitation mechanisms.

The CL from phosphor particles is a result of the statistics made up of combinations of exciting media (i.e., mobile carriers) and luminescence centers. We assume that an excited luminescence center returns to the ground state after release of one photon of CL. The number of generated CL photons in a phosphor particle is then proportional to the number of excited luminescence centers (N), which is given by the product of the exciting media (J) and the number of luminescence centers (N_L) in a given volume of phosphor particles. Accordingly, the number N is expressed by

$$N = k\,(JN_L) \tag{1}$$

where k is the proportional constant.

A most crucial point in eq 1 is a definition of the volume in which the exciting media are involved. If the exciting media do not move out of the generated place, they will uniformly distribute in the defined volume in phosphor particles. Under given electron-beam irradiation conditions, the defined volume is kept at a constant value because J is constant. On the other hand, the luminescence centers randomly and uniformly distribute at lattice sites throughout the phosphor particles, and they do not move out of their own lattice position during the luminescence process. Since the number of luminescence centers in the phosphor particles changes with N_L, the only variable in eq 1 is the concentration of N_L. If the CL intensity from phosphor screens is measured as a function of N_L, it is expected to be proportional to the concentration (mole fraction) of the luminescence center in the phosphor particle. This is the so-called concentration dependence (CD) curve of CL intensities. According to eq 1, the slope of the CD curve, plotted on a log−log scale, is expected to be unity in the region at which the concentration quenching of the luminescence intensity does not take place. This is really the case under the direct excitation, as shown below.

If mobile carriers are involved in the generation of CL and the luminescence centers act as recombination centers for them, the migration length of the mobile carriers changes with the concentration of luminescence centers. There are two different volumes for the mobile carriers: one is the variable volume, defined by the migration length of the mobile carriers, and the other is the constant volume, in which the migration length is limited to the size of the phosphor particles.[37] Therefore, the CD curves of CL stimulated by mobile carriers have two different slopes, depending on whether the volume is determined by the particle size (e.g., low concentration of luminescence centers) or the migration length (e.g., high concentration of luminescence centers). For the experiments generating CD curves for the mobile carriers, the phosphor powders should have a narrow distribution of particle sizes, with a single shape of particles.

Figure 11 shows the CD curves plotted on a log−log scale, measured under the direct excitation of luminescence centers (A) and the indirect excitation by mobile carriers (B).[37] As expected from the above consideration, it is clearly seen that there is a distinguishable difference between curves A and B. Therefore, we can use the CD curves to study the excitation mechanisms of luminescence centers in phosphor particles.

The study of CD curves reveals that plasmon and charge-transfer excitations belong to the category of the direct excitation, as pointed out in ref 37. This study further provides compelling evidence that the CL of practical phosphors is due to the recombination of electron−hole pairs (i.e., mobile carriers in the host crystals), which are generated by the irradiation of incident electrons. Figure 12 illustrates a recombination model of an electron−hole pair at a luminescence center, from which a photon of CL is emitted. The existence of the recombination mechanism has also been confirmed from a different experiment, in which mobile carriers are generated in the host crystals.[38]

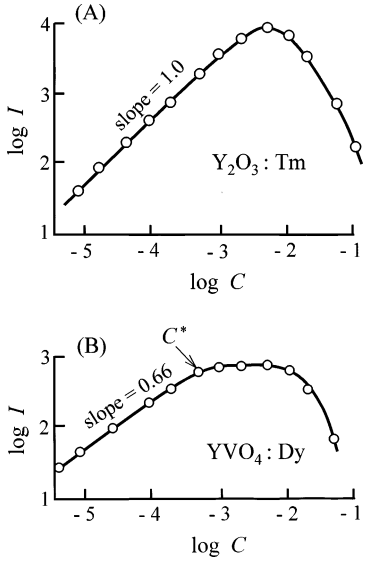

Figure 11. Log−log plot of the CL intensity I (arbitrary units) against the activator concentration C (mole fraction), i.e., the CD curve, measured under different excitation mechanisms of luminescence centers by incident electrons. (A) The CD curve taken by direct excitation of luminescence centers in Y_2O_3:Tm has a slope of unity. At $C > 0.01$, concentration quenching takes place. (B) The CD curve taken by recombination of mobile electron−hole pairs at luminescence centers in YVO_4:Dy has a slope of less than unity and exhibits a discontinuity at C^*, which shows the crystal size effect due to migration of mobile carriers.

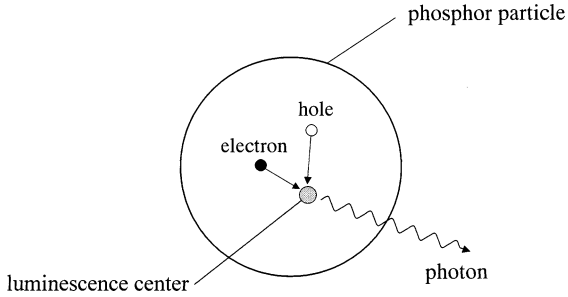

Figure 12. Model of generation of a CL photon by the recombination of an electron−hole pair. The high-energy electrons are absorbed by the host phosphor particle and form a large number of electron−hole pairs. One of these pairs reaches a luminescence center, from which a CL photon is emitted.

4. Formation of Luminescence Centers in Phosphor Crystals

There are two kinds of luminescence centers in practical phosphors: one is donor−acceptor (D−A) pair recombination centers, and the other is rare-earth recombination centers. Blue and green light from ZnS phosphors originates from D−A pair recombination centers. Red Y_2O_2S phosphor emits luminescence lines caused by the electronic transitions between the shielded levels in rare-earth ions.

4.1. Donor–Acceptor Pair Recombination Centers

To discuss optical and electrical properties of ZnS crystals, a band model, consisting of the valence band and the conduction band, has generally been used. A brief discussion of the origin of the band model of ZnS crystals is given below.

4.1.1. Band Model of ZnS

If ZnS is formed with a purely ionic bond (actually, one-half ionic bond and one-half covalent bond[39]), the formation of Zn and S elements can be written as

$$Zn(3d^{10}4s^2) + S(3s^23p^4) \rightarrow Zn^{2+}(3d^{10}4s^0) + S^{2-}(3s^23p^6) \quad (2)$$

It is known that the conduction band is composed of the empty level of $4s^0$ of Zn^{2+}, and the valence band is formed by the filled level of $3p^6$ of S^{2-}.[39] The magnitude of the energy separation between the two bands periodically varies with the lattice. This can be projected on a two-dimensional plane, i.e., configurational coordinate model, as schematically illustrated in Figure 13A. For a direct band-gap material such as ZnS, both the bottom of the conduction band and the top of the valence band in the configurational coordinate model are placed at $K = 0$, with the band-gap energy E_g. Two-dimensional expansion of the configurational coordinate model at $K = 0$ gives the band model illustrated in Figure 13B.

According to the band model of ZnS, the excitation of host lattice is explained as follows. Under irradiation with particles of energy greater than E_g, electrons belonging to the S $3p^6$ state move to the Zn $4s^0$

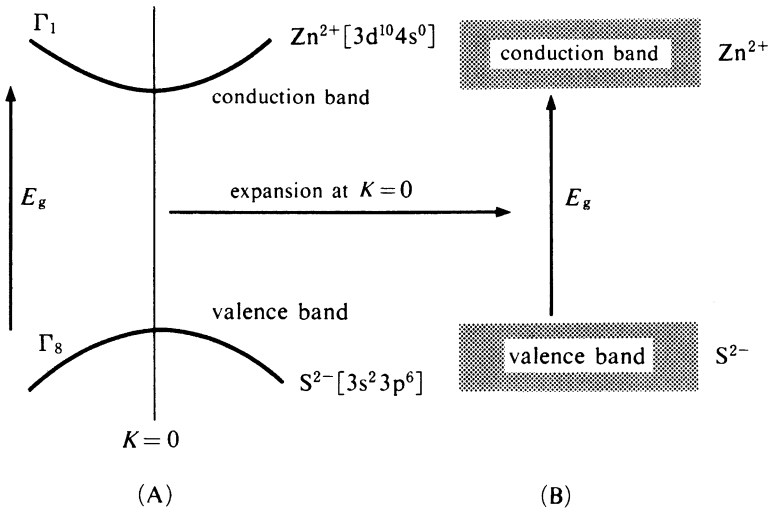

Figure 13. (A) Configurational coordinate model of ZnS. (B) Band model that is expanded at $K = 0$ in (A).

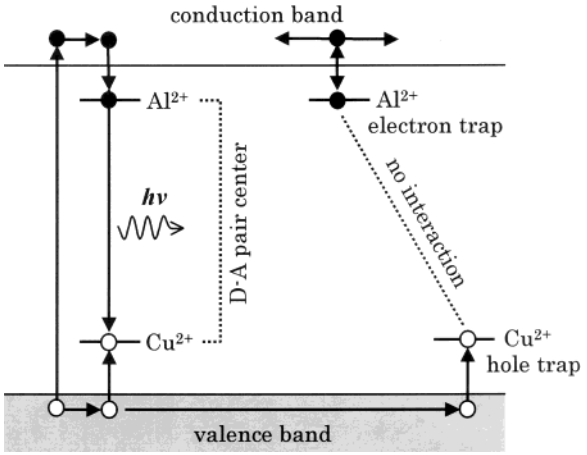

Figure 14. Illustration of a D−A pair recombination center and a non-interacting D and A center.

state, leaving holes in the valence band. From the viewpoint of an atomic model, it can be said that the excited electrons migrate only through the Zn^{2+} lattice sites, and do not move to the S^{2-} lattice sites. This leads to the idea of hopping migration of free electrons to cations and of free holes to anions in the ZnS lattice.

4.1.2. Luminescence Spectra of ZnS Phosphors

The most extensively and systematically studied ZnS phosphor is ZnS:Cu:Al,[39] although the phosphors of practical interest are (Zn,Cd)S:Ag (or Cu):Cl (or Al). In ZnS:Cu:Al phosphors, an acceptor is formed by Cu^+ 1.1 eV above the valence band, and a donor is formed by Al^{3+} 0.03 eV below the conduction band. Al^{3+} ions are substituted by Cl^- ions.

A hole generated in the valence band is captured by Cu^+ (acceptor), which becomes Cu^{2+}.[40] The Al^{3+} (donor) captures an electron, becoming Al^{2+}. If Cu^{2+} and Al^{2+} are placed within an appropriate distance for the interaction, both form an excited D−A pair, which can generate luminescence by the transition of an electron from Al^{2+} to Cu^{2+}. If an Al^{2+} ion is placed at a far distance from a Cu^{2+} ion, the two ions cannot interact with each other, and remain as electron and hole traps, respectively. Figure 14 illustrates a radiative D−A pair recombination center and non-interacting D and A centers. Recombination luminescence of D−A pairs was first found for GaP:Si:S by Bell Lab's group.[41]

The energy of the D−A pair recombination transition varies with their separation distance r. The emitted photon energy $E(r)$ is given by[42,43]

$$E(r) = E - (E_D + E_A) + \frac{e^2}{\epsilon_0 r} \qquad (3)$$

where E_D is the depth of the D level below the conduction band, E_A the depth of the A level above the valence band, and ϵ_0 the dielectric constant.

Both D and A ions distribute at random in ZnS crystals. The number of possible combinations of D−A pairs is proportionate to N^3, where N is the number of the lattice sites from the A ion (i.e., acceptor which has captured a hole). The transition probability (that the D−A pair is emissive) restricts

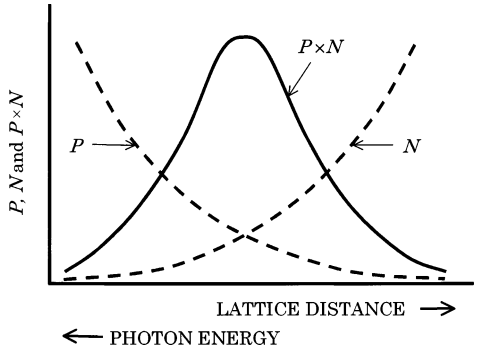

Figure 15. Number of lattice sites N and the transition probability P as a function of the separation distance, and the luminescence spectrum $P \times N$ as a function of the photon energy. The relationship between the separation distance and the photon energy is given by eq 3.

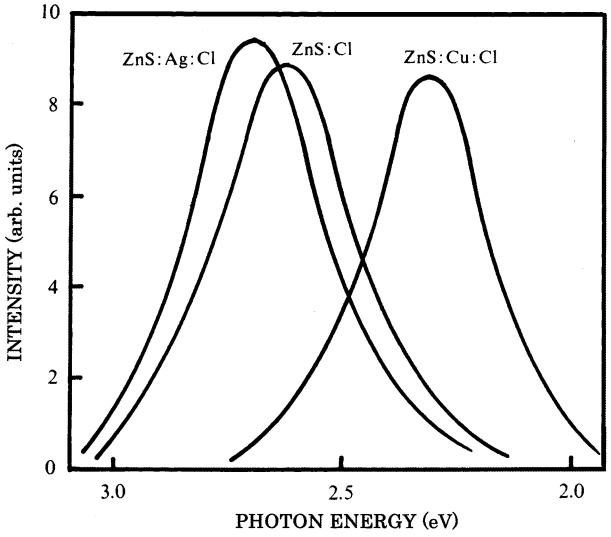

Figure 16. CL spectra of ZnS:Ag:Cl, ZnS:Cl, and ZnS:Cu:Cl phosphors under irradiation by steady 10-kV electron beam with current density of 1 μA/cm^2. The spectra have been corrected for the spectral response of the detection system.

the maximum interaction distance. The transition probability, which is an inverse function of the lifetime (holding time) of the excited state, decreases as the separation distance increases.[39,43] Figure 15 quantitatively illustrates the number N of lattice sites and the transition probability P as a function of the separation distance. In this figure, the luminescence spectrum, which is expressed by $P \times N$, is also depicted as a function of the photon energy.

Since recombination is allowed for D−A pairs which have interacted with various distances and directions, the luminescence spectrum due to D−A pair recombination (i.e., the distribution of the energy of emitted photons, corresponding to the distribution of the separation distance of D−A pairs) should be a broad band which is less temperature-dependent.[44] Figure 16 shows three CL spectra of ZnS:Ag:Cl, ZnS:Cl, and ZnS:Cu:Cl phosphors excited steadily with a 10-kV electron beam with a current density of 1 μA/cm^2.[37] All the spectra are expressed well by a bell shape (Gaussian,) with the full-width at half-maximum (fwhm) of 0.33 eV. The fwhm was almost independent of the temperature of samples (liquid N_2 and room temperatures), indicating that the lumi-

nescence is, indeed, due to D−A pair recombinations. Narrow lines due to D−A pair recombination were not observed, even at liquid N_2 temperature. It is supposed that the luminescence lines due to individual D−A pair recombination are broadened by strong electron−phonon coupling in ZnS crystals.[39]

Since the spectra are fitted by a Gaussian function, the number $f(N)$ of D−A pairs at a given separation distance r is described as[39]

$$f(N) = \frac{1}{(2\pi\sigma)^2} \exp[-(E - E(r))^2/2\sigma] \qquad (4)$$

where $E = E_g - (E_D + E_A)$. Equation 4 indicates that the number of D−A pairs with different separation distance r is symmetrically distributed around $E(r)$. The maximum interaction distance between A and D can be estimated from the fwhm of the spectra in Figure 16. The estimated value is about 500 Å. A spherical volume of 500-Å radius corresponds to the 100-lattice distance, by taking the lattice constant (5.4 Å) of cubic ZnS into account. It follows that nearly 10^3 D−A pairs exist within this sphere. Therefore, ZnS phosphor particles have very high probability to form D−A pair recombination centers.

4.1.3. Decay Curves

The lifetime (intrinsic holding time) of the excited state of the D−A pair recombination centers has been investigated experimentally. Luminescence intensity at time t after the excitation is expressed by

$$I(t) = I_0 \exp(-t/\tau) \qquad (5)$$

where I_0 is the intensity at $t = 0$ and τ is the lifetime.

A study of the decay curve of ZnS phosphors has been made under irradiation of a single electron from tritium (^{3}H). Tritium emits β-rays (electrons) with a maximum energy of 18 keV (average energy, 3.5 keV). An incident electron generates about 10^3 electron−hole pairs along its trajectory.[45] The experiments were conducted by placing a single phosphor particle of ZnS:Cu:Cl in HTO solution (50 mL),[46] where T, H, and O are tritium (^{3}H), hydrogen, and oxygen, respectively. The decay curve is plotted on semilogarithmic paper in Figure 17. The lifetime of

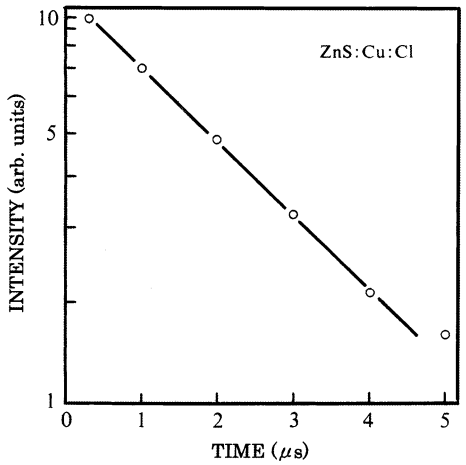

Figure 17. Decay curve of CL emitted from ZnS:Cu:Cl particles under irradiation of electrons from tritium.

the D−A pair recombination centers indeed follows eq 5, with $\tau = 2.1$ μs.

The same phosphor powder as that used in Figure 17 was mounted in a demountable CRT device. The decay curve of CL was measured under irradiation of an electron beam (10 kV, 1 μA/cm^2).[47] The decay time was 70 μs at 1/10 of the initial intensity. Furthermore, it was found that eq 5 is not applicable to the decay curves of CL when stimulated under regular excitation conditions (25 kV, 400 μA/cm^2). The decay curves of CL are in accordance with the bimolecular reaction process, which is expressed by t^{-n}. This result suggests that the electrons trapped in isolated donors (electron traps) are involved in the D−A pair recombination process, probably, tunneling recombination mechanism.

4.2. Rare-Earth Recombination Centers

Since the early 20th century, it has been know that crystals containing a small amount of rare earths emit characteristic luminescence lines, not bands, in the visible spectral region when the crystals are irradiated under an electron beam, ultraviolet light, and X-rays. The luminescence lines are assigned to the radiative transitions in the $4f^n$ shell of rare-earth ions, which are well shielded electrically with the electrons in the 5d and 6s shells. Because of line luminescence, rather than broad band, scientists paid attention to the crystal field effect, e.g., Stark effect, on rare-earth luminescence. In that time, purification of rare earths was difficult. Rare earths are chemically very close to each other, so that ordinary techniques of analytical chemistry could not separate one from the other. Hence, no one believed that rare-earth phosphors had a potential for industrial use.

After World War II, a breakthrough occurred in the purification of rare earths. A chromatographic technique using a special resin was developed in the field of atomic energy. As a result, the study of rare-earth compounds became more popular, but it was far from applications for industrial use. In the early 1960s, laser action was invented. Many scientists turned considerable attention to rare-earth ions in solids because of their multilevel splitting by the Stark effect.[48,49] They believed that rare-earth ions in solids have a great possibility for laser action, such as ruby, at room temperature. In the late 1960s, Levine and Palilla[50] proposed the use of YVO_4:Eu (laser material) as a phosphor for the red primary in color TV picture tube screens. They claimed improvement of brightness and color fidelity of the screen, thus opening the door for industrial use of yttrium oxide (Y_2O_3) and europium oxide (Eu_2O_3), and subsequently other rare earths. The red primary phosphor shifted from YVO_4:Eu to Y_2O_3:Eu, Gd_2O_3:Eu, and finally Y_2O_2S:Eu. It is believed by phosphor producers that brighter phosphor may be obtained from pure raw material Y_2O_3, in which main rare-earth impurities are Dy and Tb. Improved purification techniques will lead to better detection of impurities. Followings are the results of a systematic study conducted on the characterization of the rare-earth luminescence in solids.[37]

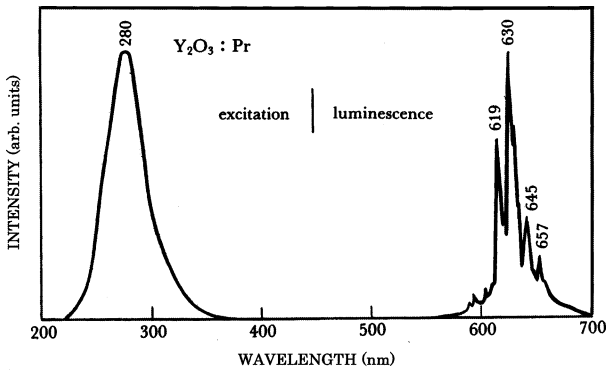

Figure 18. Luminescence and excitation spectra of Y_2O_3: Pr phosphors.

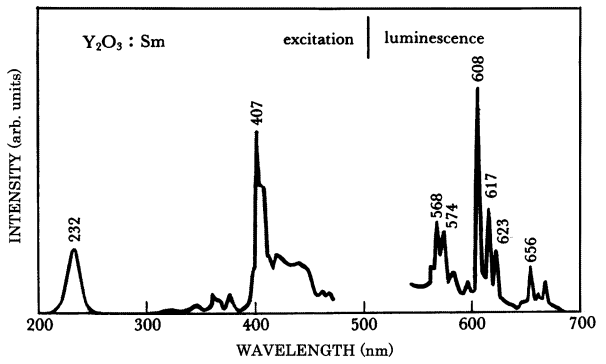

Figure 19. Luminescence and excitation spectra of Y_2O_3: Sm phosphors. The luminescence was observed under excitation with 360-nm photons.

4.2.1. Luminescence Spectra of Y_2O_3 Phosphors

Nine rare earths (REs) emit characteristic luminescence lines under irradiation with electron beams and with photons of energies greater than 2 eV (>600 nm): Pr^{3+}, Sm^{3+}, Eu^{3+}, Gd^{3+}, Tb^{3+}, Dy^{3+}, Ho^{3+}, Er^{3+}, and Tm^{3+}. The other REs (except for Nd and Yb, which emit infrared luminescence) have no luminescence in the visible or near-ultraviolet region. The recorded, not energy-corrected, luminescence and excitation spectra of the nine REs in Y_2O_3 are shown in Figures 18−27. The concentration of REs in all cases is about 0.001 mole fraction. One can see a sharp difference in the energy distribution, resulting in the characteristic luminescence color depending on the RE ions. These spectra are in fairly good agreement with those reported by many researchers.[51−53] Assignments of the electronic transitions of the luminescence and excitation lines have been done on the basis of the energy diagram by Dieke and Crosswhite.[54] The luminescent properties of respective RE ions are as follows:

Figure 18 shows the luminescence and excitation spectra of Y_2O_3:Pr. An intense red luminescence is observed under the excitation with 280-nm light and electron beam. The luminescence spectrum consists of a number of lines in the vicinity of the 630-nm line. The spectral shape is not changed by the direct excitation of the $^3P_0$ and $^3P_1$ states in Pr^{3+} ions. On the other hand, no luminescence is observed with the direct excitation of the $^1D_2$ state in Pr^{3+}. From these results, it is supposed that the luminescence lines around 630 nm originate from the electronic transitions $^3P_0 \rightarrow {}^3H_6$ and $^3P_0 \rightarrow {}^3F_2$.[55] The excitation spectrum in Figure 18 has a broad and strong band peaking at 283 nm (f−d transition) and some weak lines in the range between 452 and 499 nm (not shown here). They are assigned to the electronic transitions from the ground state, $^3H_4$, to the four excited states, $^3P_2$, $^1I_6$, $^3P_1$, and $^3P_0$, in Pr^{3+} ions.

Figure 19 shows the luminescence and excitation spectra of Y_2O_3:Sm. The luminescence spectrum consists of three groups of lines in the regions near 568, 608, and 656 nm, which are assigned to the electronic transitions from the lower emitting $^4G_{5/2}$ state to the $^6H_{5/2}$, $^6H_{7/2}$, and $^6H_{9/2}$ states in Sm^{3+} ions, respectively. The relative line intensity largely depends on the exciting wavelength. Figure 19 is obtained under irradiation with 360-nm light (charge-transfer band), where the 608-nm line is predominant. The intensity of the 565-nm line becomes most intense if the phosphor is irradiated with 230-nm light (see Figure 20). This difference in the luminescence spectrum with exciting radiation is probably due to the selective excitation of Sm^{3+} ions that are occupying two different lattice sites.

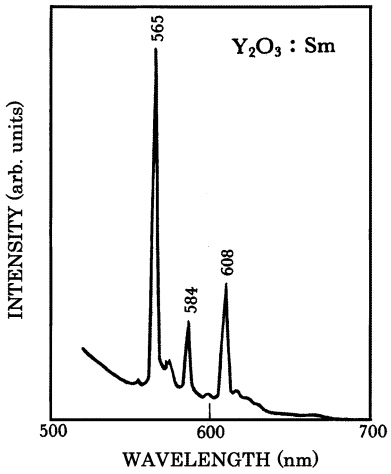

Figure 20. Luminescence spectrum of Y_2O_3:Sm phosphors excited with 230-nm photons.

We present the luminescence and excitation spectra of Y_2O_3:Eu in Figure 21. The spectra agree with those reported by Chang[51,52] and by Ropp,[53] who are pioneers in the Y_2O_3:Eu study. The most intense single luminescence line, which is ascribed to the transition $^5D_0 \rightarrow {}^7H_2$, appears at 611 nm. The excita-

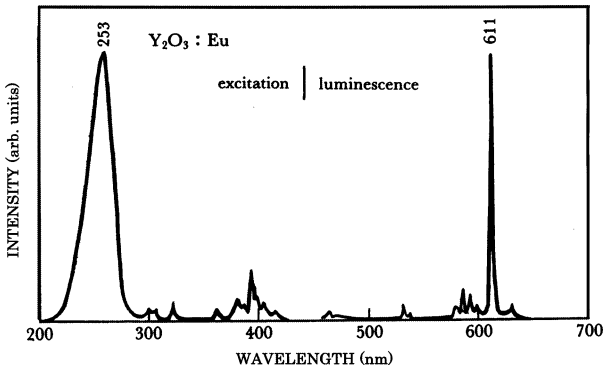

Figure 21. Luminescence and excitation spectra of Y_2O_3: Eu phosphors.

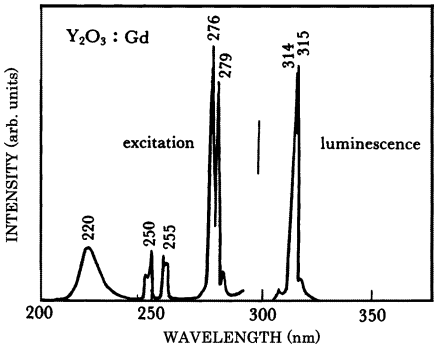

Figure 22. Luminescence and excitation spectra of Y_2O_3: Gd phosphors.

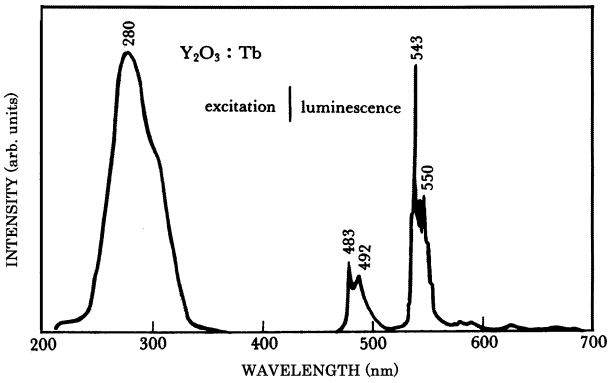

Figure 23. Luminescence and excitation spectra of Y_2O_3: Tb phosphors.

tion spectrum for this luminescence consists of a broad band peaking at 253 nm and a number of small and narrow lines around 400 nm. The former could be assigned to the charge-transfer band. The latter is ascribed to the transitions within the $4f^6$ configuration of Eu^{3+}.

In Figure 22 is shown the luminescence and excitation spectra of Y_2O_3:Gd. The main luminescence line appears at 315 nm.[56] This line splits into four lines: 309, 314, 315, and 318.5 nm. The luminescence lines at 314, 315, and 318.5 nm are assigned to the transitions $^6P_{7/2} \rightarrow {}^8S_{7/2}$, and the line at 309 nm to the transition $^6P_{5/2} \rightarrow {}^8S_{7/2}$. The excitation spectrum consists of a broad band at 220 nm and a number of lines in the long-wavelength region. The former is assigned to the charge-transfer band. The latter is the direct excitation lines of Gd^{3+}, i.e., from the ground state $^8S_{7/2}$ to the excited state $^6I_{7/2}$ for 282 nm, to $^6I_{9/2}$ for 279 nm, to $^6I_{11/2}$ for 276.5 and 274 nm, to $^6D_{7/2}$ for 255 nm, and to $^6D_{3/2}$ and $^6D_{5/2}$ for 247−248 nm, respectively.

Figure 23 shows the luminescence and excitation spectra of Y_2O_3:Tb. The luminescence spectrum consists of a series of groups of lines in the regions near 483, 543, 583, 623, and 666 nm. They are ascribed to the electronic transitions from the lowest excited state $^5D_4$ to the multiple ground state ^7F_j ($j = 3-6$) in Tb^{3+}. The intensities of the groups at 623 and 666 nm are very weak, below 1/100 of that of the main line at 543.5 nm. The relative intensities of these lines change to some extent with Tb concentration. Such a change is likely linked to the fact that Tb^{3+} ions occupy two sites with different symmetries in Y_2O_3. The luminescence lines arising from another

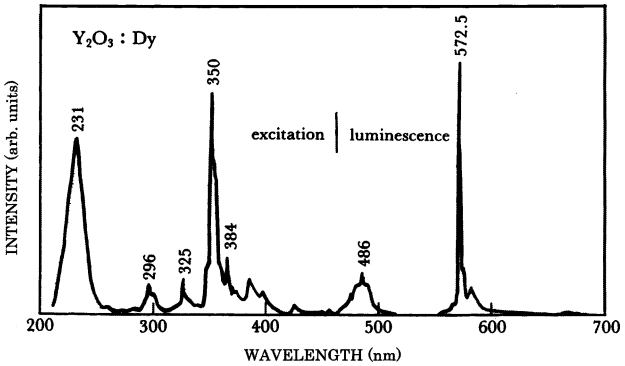

Figure 24. Luminescence and excitation spectra of Y_2O_3: Dy phosphors.

excited state $^5D_3$ have not yet been detected in Y_2O_3: Tb. The excitation spectrum for the green luminescence at 543 nm is composed of two broad bands at 280 and 304 nm.

Figure 24 shows the luminescence and excitation spectra of Y_2O_3:Dy. The main luminescence line is located at 572.5 nm. This line, as well as a weak line around 580 nm, could be attributed to the transitions $^7F_{9/2} \rightarrow {}^6H_{13/2}$ in Dy^{3+}. On the other hand, the lines at around 486 nm are attributed to the $^7F_{9/2} \rightarrow {}^6H_{15/2}$ transition. No change of the luminescence spectrum is observed, even if the Dy concentration and the excitation wavelength are changed. The luminescence color is always yellow. The excitation spectrum for the 572.5-nm luminescence consists of a broad band at 231 nm (charge-transfer band) and many lines in the long-wavelength region (transitions within Dy^{3+} ions).

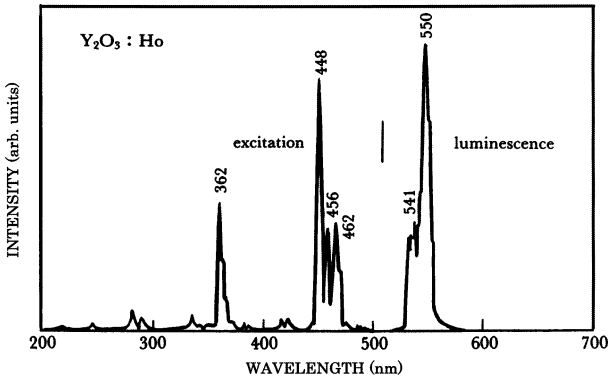

Figure 25. Luminescence and excitation spectra of Y_2O_3: Ho phosphors.

Figure 25 presents the luminescence and excitation spectra of Y_2O_3:Ho. The luminescence lines around 545 nm are assigned to the transitions $^7F_4 \rightarrow {}^5I_8$ and $^5S_2 \rightarrow {}^7I_8$. The excitation spectrum detected at 550 nm is composed of a large number of lines from the ultraviolet to blue region. They are attributable to the transitions of $4f^{10}$ in Ho^{3+} ions.

Figure 26 shows the luminescence and excitation spectra of Y_2O_3:Er. The luminescence spectrum has a large number of lines around 552 nm, which are attributed to two transitions, $^2H_{9/2} \rightarrow {}^4F_{13/2}$ and $^4S_{3/2} \rightarrow {}^4I_{15/2}$, in Er^{3+} ions. It is very difficult to separate the two transitions because they overlap with each other in the energy diagram. The strong excitation

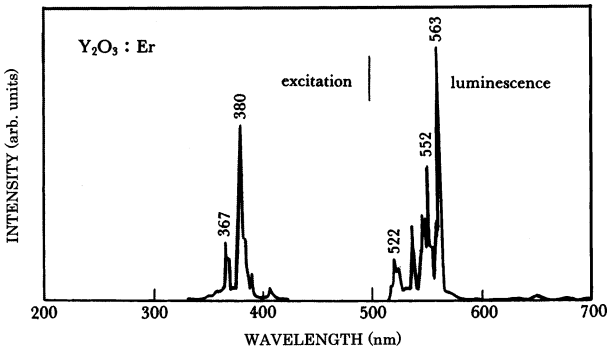

Figure 26. Luminescence and excitation spectra of Y_2O_3: Er phosphors.

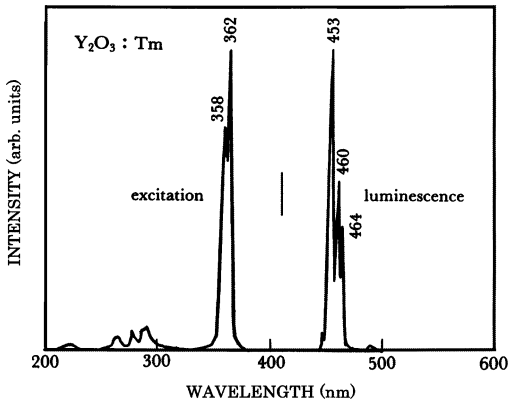

Figure 27. Luminescence and excitation spectra of Y_2O_3: Tm phosphors.

lines around 380 nm are ascribed to the transitions from the $^4I_{15/2}$ state to the $^4G_{11/2}$ state.

Figure 27 shows the luminescence and excitation spectra of Y_2O_3:Tm. This material emits blue luminescence lines at 453, 460, and 464 nm. They are assigned to the radiative transitions $^1D_2 \rightarrow {}^3F_4$. The excitation spectrum for the 453-nm luminescence exhibits two intense lines at 358 and 362 nm, arising from the optical transitions within Tm^{3+} ions.

4.2.2. Luminescence Spectra of Other Oxide Phosphors

REs in cubic Gd_2O_3 exhibit almost the same luminescence and excitation spectra as those in Y_2O_3. However, Gd_2O_3 has another crystal phase, i.e., monoclinic structure. Monoclinic Gd_2O_3 brings about a change in crystal field surrounding the RE ion, resulting in slightly different spectra from those of cubic Gd_2O_3. The phase transition temperature lies at 1250 °C, above which the monoclinic structure is stable. Figure 28 shows the luminescence spectra of Eu^{3+} in Gd_2O_3 fired at 1200 and 1300 °C.[37] The lines of both spectra are similar in the wavelength region, but their relative intensities are different. The intensity of monoclinic Gd_2O_3 is generally weak compared with that of cubic Gd_2O_3.

As a typical example of other RE-activated phosphors, the luminescence and excitation spectra of Y_2O_2S:RE^{3+} are shown in Figures 29−36.[37]

In summary, the REs in Y_2O_3, Gd_2O_3, La_2O_3, Y_2O_2S, La_2O_2S, and YVO_4 exhibit characteristic luminescence and excitation lines in their spectra. From a comparison of Figures 18−27 with Figures 29−36, it is recognized that the line positions are, in general, less dependent on the host crystals. Therefore, the luminescence color of the RE-activated phosphors strongly depends on the RE ions used. Eu^{3+}, Sm^{3+}, and Pr^{3+} are used for red, Tb^{3+}, Ho^{3+}, and Er^{3+} (and in some crystals Pr^{3+}) for green, Tm^{3+}

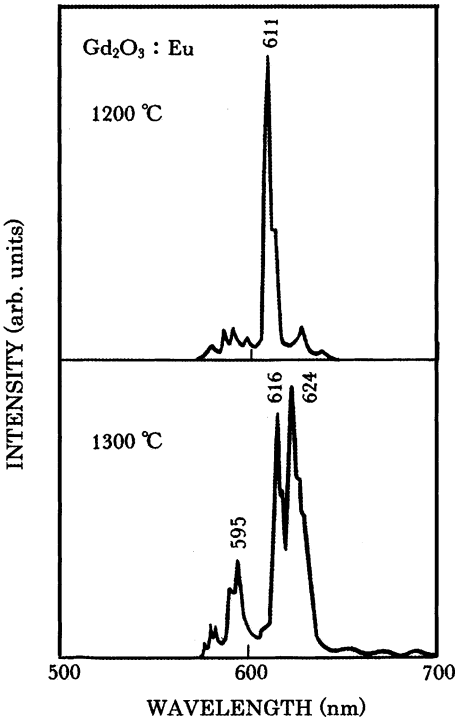

Figure 28. Luminescence spectra of Gd_2O_3:Eu phosphors fired at 1200 and 1300 °C.

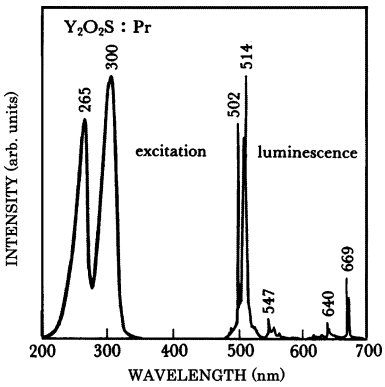

Figure 29. Luminescence and excitation spectra of Y_2O_2S: Pr phosphors

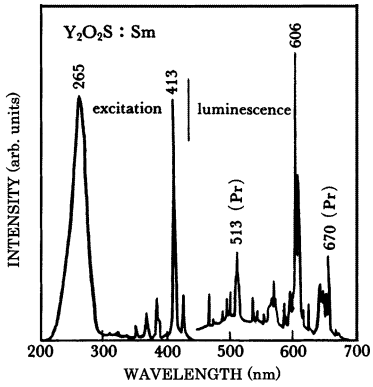

Figure 30. Luminescence and excitation spectra of Y_2O_2S: Sm phosphors.

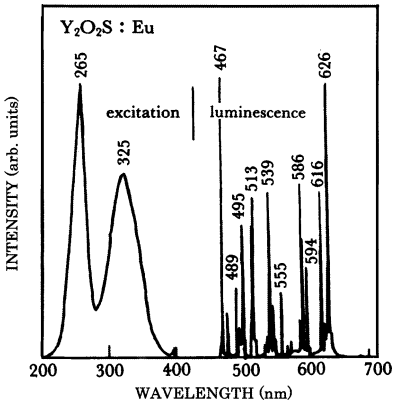

Figure 31. Luminescence and excitation spectra of Y_2O_2S: Eu phosphors.

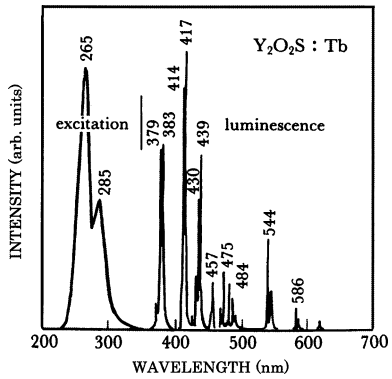

Figure 32. Luminescence and excitation spectra of Y_2O_2S: Tb phosphors.

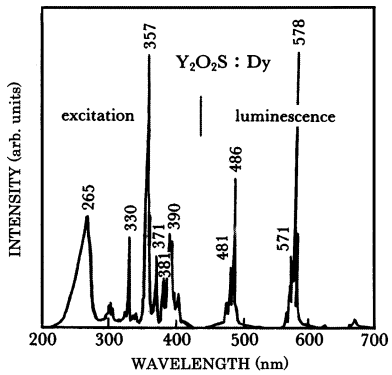

Figure 33. Luminescence and excitation spectra of Y_2O_2S: Dy phosphors.

for blue, and Gd^{3+} for ultraviolet. Hence, we can roughly choose the rare-earth activators suitable for different luminescence colors.

4.2.3. Decay Curves

Figure 37 represents the decay curves of CL of Y_2O_3:RE^{3+}.[37] The excitation was done by irradiation with a pulsed electron beam of 10 keV. The curves exhibit a single-exponential decay (i.e., monomolecular type), except for Ho. That is, they follow eq 5. This clearly indicates that the decay curve is determined only by the conditions of RE ions in Y_2O_3 crystals. According to the decay times determined, the REs can be classified into two groups: one group is Tb, Dy, and Sm ($\tau \approx 2$ ms), and the other is Eu, Ho, and Pr ($\tau \approx 0.5$ ms). The decay time of CL from REs in

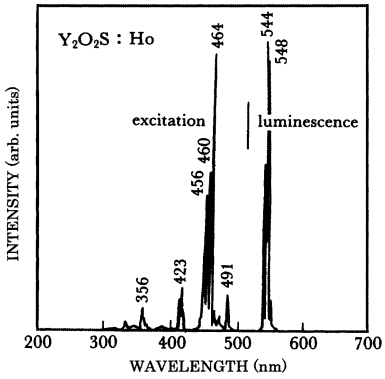

Figure 34. Luminescence and excitation spectra of Y_2O_2S: Ho phosphors.

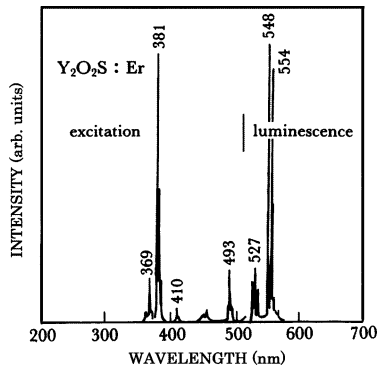

Figure 35. Luminescence and excitation spectra of Y_2O_2S: Er phosphors.

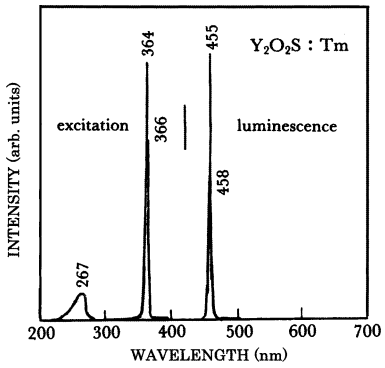

Figure 36. Luminescence and excitation spectra of Y_2O_2S: Tm phosphors.

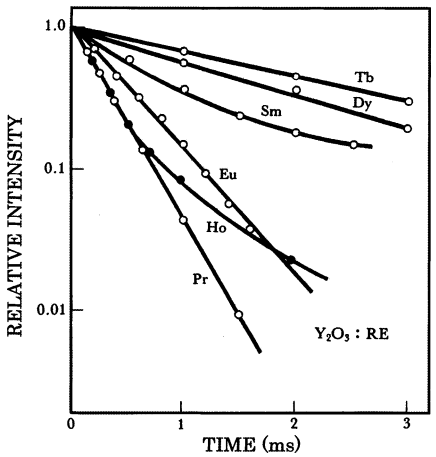

Figure 37. Decay curves of CL in Y_2O_3:RE^{3+}, where RE^{3+} is Tb, Dy, Sm, Eu, Ho,, and Pr.

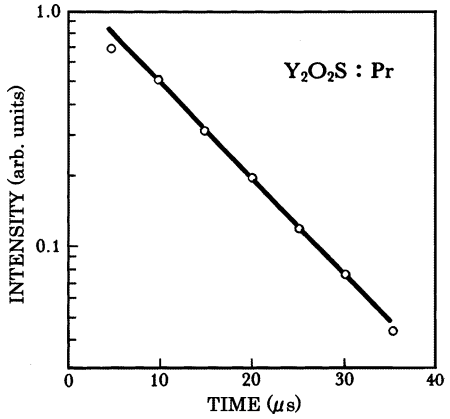

Figure 38. Decay curve of CL in Y_2O_2S:Pr phosphors.

Y_2O_3 may be related to the depth of trap levels, which are able to capture conduction electrons. In general, the wave function is localized in the deeper trap ion. This makes the optical transition probability higher, leading to a faster decay rate.

In Figure 38 is shown the decay curve of Y_2O_2S:Pr phosphors under cathode ray excitation.[37] The decay can also be described by a single exponent. One gets $\tau = 10.5\ \mu$s, which is shorter than those in Y_2O_3:RE^{3+} phosphors.

5. Optimized Energy Conversion Efficiencies of CRT Phosphors

Under irradiation with an electron beam, a large number of inorganic compound crystals emit characteristic CL in the visible region, which is caused by doped chemical ions, i.e., activators or luminescence centers. Different host crystals with the same activator ions exhibit different luminescence efficiencies. The variation in luminescence efficiency has been ascribed to the difference in the probability of the energy transfer of radiation-induced carriers to activator ions. As described in section 3, many excitation mechanisms of CL, involving free carriers,[57] plasmons,[58,59] and excitons,[60] have been proposed. Several attempts to explain the CL mechanisms have been made,[61−65] but no solid confirmation has been achieved. This is one reason that CL technology still remains as an arcane one. In practice, phosphor pixels are merely an energy converter from invisible electrons to visible photons. This has led some workers[58,59,66−68] to an estimation of the energy conversion efficiencies in commercial phosphors.

The energy of CL (E_{CL}) generated in phosphor pixels can be expressed by

$$E_{CL} = \eta W_{irrad} \tag{6}$$

where η is the energy conversion efficiency of CL generated by the irradiation with incident electrons of energy W_{irrad}. The energy efficiency (W/W), rather than the lumen efficiency (lm/W), should be considered in the study of CL. Some display researchers have directed their attention to an improvement of the lumen efficiencies since the 1980s.[69] The lumen efficiency is uniquely determined from the spectral distribution of CL, and corresponds to the brightness. It is, therefore, not suitable for discussions of the conversion efficiency.

Table 2. Energy Conversion Efficiency η and Band-Gap Energy E_g of Practical Phosphors

phosphor	η (%)	ref	E_g (eV)	ref
ZnS:Ag:Cl (blue)	23	72	3.9	74
ZnS:Cu:Al (green)	19−21	58,59	3.9	74
Y_2O_2S:Eu (red)	13	58,59	6.7	75
Y_2O_3:Eu (red)	8.7	73	6.7	76
YVO_4:Eu (red)	8	67	5.6	77
Zn_2SiO_4:Mn (green)	8	67	5.5	78

The value of η in phosphor particles changes with the combination of host crystal and activator ion, even after the activator concentration has been optimized. Many host crystals inevitably contain a trace amount of transition elements as impurities. The host crystal for practical phosphor is empirically selected from many materials by trial and error.[2] Recent experimental results on phosphors are summarized in refs 70 and 71.

According to Laporte's rule, optical dipole transitions are allowed only between electronic states of different parity. For instance, a ground state of odd parity is reached by emission of a photon from an even-parity excited state, and vice versa. This parity selection rule is removed when the luminescence centers locate at the lattice sites that lack a center of inversion symmetry. The probability of the allowed electronic transitions in an asymmetric field is extremely high as compared with that in a symmetric field.[71] All of the host crystals used as commercial phosphor particles do not have inversion symmetry. This is a reason that the commercial phosphors have high η values. For instance, the η values of CL of blue and green ZnS phosphors are 19−23%, and other commercial phosphors have $\eta = 8$−13%, as listed in Table 2. It is worth noting that the values of η in Table 2 have not changed during the past three decades.

The reported values of η can be confirmed on the basis of a simple energy flow model. From the experimental results of mobile carriers generated by means of electric current,[79] it has been found that the generation energy of electron−hole pairs in phosphor crystals is approximated as $3E_g$, where E_g is the band-gap energy. By using this approximation, the number of pairs N_{pair} generated in a given phosphor particle under irradiation by an electron can be estimated. If an incident electron has an energy of 25 keV, typical in many applications, N_{pair} is expressed as follows:

$$N_{pair} = 25\ \text{keV}/3E_g \tag{7}$$

Since the band-gap energy E_g of cubic ZnS phosphor crystal is 3.9 eV,[74] we get

$$N_{pair} = 2137 \tag{8}$$

In ZnS phosphor,[80] the luminescent centers are formed as D−A pairs, and one photon is emitted by the recombination of an electron−hole pair at the D−A pair center. Therefore, it can be said that the

ZnS phosphor crystal generates 2137 photons of CL by one incident electron of 25 keV.

The above number, 2137, is confirmed from the energy conversion efficiency η, which was determined from the energy measurement by thermopiles.[58,59] The green ZnS phosphors have $\eta \approx 20\%$. When the incident electron has an energy of 25 keV, the converted energy for generation of CL photons is evaluated to be 5 keV. The average energy of the green light (530 nm peak) is 2.3 eV. Then, the average number of CL photons N_{photon} is calculated as

$$N_{photon} = 5000 \text{ eV}/2.3 \text{ eV} = 2174 \quad (9)$$

This number of 2174 photons is in excellent agreement with that due to the recombination of electron−hole pairs (2137).

From the agreement mentioned above, it is concluded that CL photons in the practical phosphor particles are generated by electron−hole recombination at luminescence centers. In other words, phosphor producers have optimized the energy conversion efficiencies of the commercial phosphors practically.

6. Appropriate Number of Photons Emitted from Phosphor Pixels in CRTs in Illuminated Rooms

The images on CRTs are illustrated by the CL light from phosphor pixels, which is the flux of visible photons. For comfortable observation of the images on CRTs which are placed in illuminated rooms, each image pixel in display devices should emit an appropriate number of photons. Although an appropriate number of photons is a matter of important concern to evaluate the display devices, there has been no report on the photon number required for comfortable observation. We find that such a number is calculable from the irradiation conditions of an electron beam on the phosphor pixels in ordinary CRTs. In practical production of CRTs, this number has been empirically determined in the past decades.

The light images on CRTs for personal computers (PCs) are usually watched in illuminated rooms. A phosphor screen in typical CRT monitors is irradiated by the electron beam, with anode voltage of 25 kV, beam current of 400 μA, and diameter on the phosphor screen (VGA resolution) of 0.8 mm. The irradiation energy (W_{irrad}) on the phosphor pixel is given as

$$W_{irrad} = (25 \times 10^3) \times (4 \times 10^{-4}) \times 10^2 = 1 \text{ kW/cm}^2 \quad (10)$$

This energy is converted to the energy of CL in phosphor pixels. Taking into account the fact that $\eta \approx 20\%$ for the green ZnS:Cu:Al phosphor,[58,59] the energy of emitted CL light (W_{CL}) is calculated as

$$W_{CL} = 0.2 \times 1 \times 10^3 \text{ W/cm}^2 = 200 \text{ W/cm}^2 \quad (11)$$

As described before, the average energy of the green light (530 nm) from ZnS:Cu:Al is 2.3 eV ($= 3.7 \times 10^{-19}$ W). The number of emitted photons N_{photon} from each phosphor pixel in the practical CRT monitors is thus obtained as

$$N_{photon} = 200/(3.7 \times 10^{-19}) = 5.4 \times 10^{20} \text{ photons/s·cm}^2 \quad (12)$$

A distance of distinct vision is about 30 cm apart from the screen. From the calculation above, it can be said that if each image pixel in the display devices for PCs emits 5.4×10^{20} photons/s·cm^2, the light images on the screens in illuminated rooms are comfortably watched at a distance of distinct vision.

On the other hand, video images of TV sets are usually watched at a distance of about 5 times the diagonal measurement of the screen. The photon number emitted from CRTs of TVs should be different from that of PCs. For example, a 25-in. color TV set is operated under the beam conditions of 30 kV anode voltage, 1 mA current, and 1 mm diameter. The irradiation energy becomes 3 kW/cm^2. Then, we get

$$N_{photon} = 1.5 \times 10^{21} \text{ photons/s·cm}^2 \quad (13)$$

That is to say, for comfortable watching of video images of TV screens in illuminated rooms, each screen pixel should emit 1.5×10^{21} photons/s·cm^2.

The calculated number of photons will provide us the criterion for evaluation of display devices for practical use. This criterion is an important conclusion of the present review.

7. Advantage of CRTs as Display Devices

Individual pixels in phosphor screens of CRTs are being bombarded with high energy density of a few kW/cm^2. If the energy conversion efficiency is 20%, 80% of the irradiation energy is converted to heat in pixels. If a screen in a CRT is irradiated with a nonscanning electron beam, it is immediately heated to the temperatures at which the phosphor crystals are seriously damaged. When the same phosphor screen is irradiated with a scanning electron beam, e.g., at the National Television System Committee, USA (NTSC), raster conditions, the irradiation duration of each phosphor pixel is short, with a repetition rate of 60 Hz. Under scanned irradiation, it has been revealed that the CL intensity increases linearly with the dumped energy of the electron beam.[81] The rise in temperature of phosphor particles is detected by measuring the ratio of the luminescence intensities between the $^5D_0$ and $^5D_1$ lines from Eu^{3+} ions in the Y_2O_2S:Eu phosphor screen. The temperature rise is only a few °C, even though the energy density is 5 kW/cm^2.[81] Such a low rise in temperature is certainly attributed to instantaneous irradiation of phosphor pixels by the electron beam.

When the entire area of the phosphor screen in a 25-in. CRT is scanned by the 1-mA electron beam with 1-mm spot diameter under the NTSC condition, the scanning electron beam has an energy of 30 W/spot ($= 30 \times 10^3$ V $\times$ 1 $\times$ 10^{-3}A/spot). The horizontal length of the screen is 50 cm, and the scanning time of one horizontal line is 63.5 μs, so the scanning speed is 7.9×10^5 cm/s. The individual phosphor pixels in a 1-mm spot size are irradiated for 127×10^{-9} s by the scanning electron beam. The dumped

Table 3. Limitation of Light Output from Various Light Sources as Display Devices

light source	efficiency (W/W)	linear range	limitation of output
tungsten lamp	~0.8%	very wide	meltdown of W filament (3410 °C)
high-brightness LED	~5%	very wide	thermal quenching (250 °C)
inorganic EL	~0.8%	narrow	electric breakdown
organic EL	1−3%	narrow	electric breakdown
fluorescent lamp	~20%	narrow	self-absorption
plasma (PDP)	<1%	narrow	heating
CL (scanning)	~20%	very wide	thermal quenching
CL (continuous)	~20%	narrow	crystal damage by heatup
LCD	fluorescent lamp, 20% filter, 5−8%	median	output of backlight and transmission of film layer

energy on each pixel is roughly estimated to be 3.8×10^{-6} W, which results in an instantaneous peak brightness of about 5×10^4 cd/m^2. On the other hand, since the area of the phosphor screen is 1875 cm^2, the irradiated energy density per unit phosphor screen area is calculated to be 16 mW/cm^2 (= 30 W/1875 cm^2). This leads to a screen brightness of 330 cd/m^2. There is a large difference, more than 2 orders of magnitude, between the instantaneous peak brightness and the screen brightness of CRTs. Since the phosphor screen of a CRT is irradiated with a rapidly scanning electron beam, its brightness should be evaluated by the instantaneous brightness of image pixels, not by the screen brightness averaged over time and screen area.

The above calculation provides us crucial and useful information for the evaluation of practical display devices. The maximum instantaneous brightness is determined from the linearity of light intensity with the input power. Table 3 shows the limitation of light output from various light sources as candidates for emissive display devices. The meltdown of a tungsten filament (3410 °C) gives the upper limitation of light output, giving the brightness from 50 to 25000 lm, depending on the input power.[82] High-brightness light-emitting diodes (HBLEDs),[83] such as GaInN,[84] can increase the energy up to 250 °C, at which thermal quenching of the luminescence begins. Inorganic EL devices are constructed with thin film layers of the thickness from nanometers to micrometers, in which the input power is limited by electrical breakdown of films.[85] This leads to a low light output from the inorganic EL devices. Organic EL displays (OELDs) are also constructed with thin films of organic layers,[86] and they have a similar story to that of inorganic ELs. Fluorescent lamps have high efficiency (about 20%) of energy conversion, but the limitation of the light output comes from self-absorption of UV light by mercury vapor, resulting in constant light output.[87] Plasma display panels (PDPs) have a low energy conversion efficiency due to the discharge of rare gases.[88] Liquid crystal displays (LCDs) are a kind of optical filter with a total transmission of about 8%, and also have the backlight (energy conversion efficiency less than 20%[89]). To obtain the appropriate brightness, LCDs must consume a large amount of power as heat. From the argument above, one can recognize that the scanning CRTs, tungsten lamps, and HBLEDs are able to achieve the appropriate instantaneous brightness of image pixels for practical use, because of the linearity of the luminance intensity in a very wide range. Among them, only CRTs realize a fine resolution of the images. Furthermore, the CRTs have another great advantage, that is, a simple addressing of phosphor pixels on the entire phosphor screen by a scanning electron beam, versus the addressing of flat panel displays (FPDs), such as LCDs, PDPs, OELDs, and so on.

8. Screenable Phosphor Powders on Faceplates of Color CRTs

We have discussed the intrinsic properties of CL from phosphor particles, which promise many advantages of CL images in CRTs. The image qualities, such as screen luminance, smearing, contrast, and flickering of images, are strongly influenced by the optical scattering of CL generated on the surface of phosphor particles involved in the screens (i.e., extrinsic properties of CL). The screenable phosphor powders will provide an optimized image quality for viewers. Several studies have been reported on the screening of phosphor powders.[90−95] These previous reports, however, do not give a clear picture of the screening of phosphor powders, and therefore the mechanisms involved remain unelucidated.

In practice, phosphor powders are screened on the faceplate of CRTs with arrangement of phosphor particles (2×10^{10} particles/g) in a screen density of 4 mg/cm^2. All phosphor particles do not have an equal size. The distribution of the particle sizes is evaluated from a statistical means. If we consider primary particles, their distribution is approximated by a log-normal function with a significant error of 5%.[96] The optical scattering in phosphor screens is related with the total surface area of phosphor particles in the screen. The total surface area is proportional to the number (n) of layers of particles, as the particles distribute with the log-normal probability. The number n is expressed by[37]

$$n = 1.65w/(\rho d^2) \qquad (14)$$

where w is the screening density of phosphor powder on the faceplate, ρ the density of phosphor particle, and d the average particle size of phosphor powder.

The optimized phosphor screens are produced after maximizing CL output and minimizing optical scattering of CL in the screen. The number of layers of optimal phosphor screen is experimentally determined to be $n = 1.5$ in the laboratory.[37] The screening of the phosphor powder with $n = 1.5$ layers, however, is a very hard task. In practical production of CRTs, the optimal phosphor screens can be made with $n =$ 2 layers.

Color phosphor screens in CRTs are produced by sequential photolithographic deposition of each color phosphor powder (blue, green, and red) on the faceplate with the desired patterns (dots or stripes).[37,94,97] Formation of patterned phosphor screens consists of two steps: (i) screening of the phosphor powder on the faceplate and (ii) sequential photolithography. To obtain an ideally patterned phosphor screen on CRT faceplates by photolithography, a uniform thickness of dried phosphor screen with $n = 2$ is highly desired.

A phosphor screen is produced on the faceplate by screening of a photosensitized slurry in which phosphor particles are dispersed. There are many photosensitized resins on the market, but PVA resin is preferred for the reason that phosphor particles are well dispersed in this slurry with a pH of about 7.0.[37] If other photosensitized resins are used, phosphor particles definitely aggregate in the slurry, even with pH = 7.

The PVA phosphor slurry is made by suspending phosphor particles in PVA solution. Because there is no means to detect the dispersed particles in the PVA phosphor slurry with high viscosity and high phosphor content, the dispersion of phosphor particles is not studied in the PVA phosphor slurry. Nevertheless, it has been believed that the phosphor particles are well dispersed in the PVA phosphor slurry, although there is no apparent reason.

The PVA phosphor slurry is deposited on the CRT faceplate by applying a spin-coat technique. After the screens are dried, photolithographic techniques are applied to the dried screens. The PVA resin itself is not photosensitive. It becomes photosensitized by addition of a small amount of ammonium dichromate (ADC). As is experienced, a difficulty in the screening of phosphor powders comes from the photosensitivity of the PVA phosphor slurry. The ADC in solution dehydrates into three segments:[98] (a) $Cr_7O_7^{2-}$, (b) CrO_4^{2-}, and (c) $HCrO_4^-$, depending on the pH values. Among them, only $HCrO_4^-$, which is present in the range $4.5 < pH < 8.0$, achieves the photosensitization of the PVA screen. It should be noted that the concentration of $HCrO_4^-$ changes sharply with a small change in pH between 5.5 and 7.5. The photosensitivity of PVA slurry drastically changes with the pH values, even though the ADC concentration added is tightly controlled. The pH value in PVA phosphor slurry must be carefully adjusted to around 7.0 for good dispersion of phosphor particles, as pointed out in ref 37.

In dried PVA phosphor screens, each phosphor particle is covered with a PVA resin film. The film (about 0.8 μm in thickness[98]) should be thick enough to cause the phosphor particle to adhere on the faceplate during the subsequent photolithographic process. The film thickness can be controlled with the mixing ratio of phosphor powder to PVA resin. For the adhesion of phosphor particles on the faceplate of CRTs, the PVA film underneath the phosphor particles ought to experience a photoreaction as a result of the absorption of irradiated UV light for polymerization of the PVA film (i.e., hardening). After the exposure with UV light passing through a patterned mask, the screen is developed with warm water to remove the unexposed area from the phosphor screen. Thus, we get the patterned phosphor screens on the faceplate.

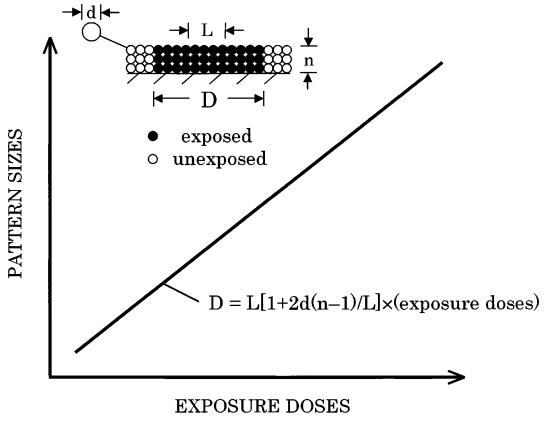

Figure 39. Pattern sizes of defect-free phosphor screens as a function of the exposure doses of UV light.

In the exposure process for adhesion, UV light must reach the bottom layer of phosphor particles in the screen. Since the phosphor particles have a large refractive index, UV light is scattered efficiently by the particle surfaces. If the PVA resin film covering the phosphor particles has a low absorption coefficient, UV light has a chance to reach the bottom layer. This requires a low concentration of ADC in the PVA phosphor screens. The absorbance of hardened PVA resin film becomes negligible after UV light exposure.[37] As a result, the absorption of UV light does not follow Lambert−Beer's law. On the other hand, the optical absorption in the dried PVA phosphor screen obeys Bunsen−Roscow's law, so that the scattering range is linearly proportional to exposure doses. Since the scattering occurs equally in every direction, the penetration depth of UV light increases with the exposure doses. There is a threshold dose because the UV light reaches the bottom layer in a given screen, at which the patterned phosphor screens adhere on the faceplate. If the phosphor particles perfectly disperse in the PVA slurry, the pattern sizes would vary linearly with the exposure doses. The pattern size D of the adhered phosphor screen is expressed by

$$D = L[1 + 2d(n - 1)/L] \tag{15}$$

where L is the diameter of incident light (see the inset in Figure 39). Since an ideal phosphor screen is made with $n = 2$, the minimum pattern size of an adhered phosphor screen is given as

$$D = L + 2d \tag{16}$$

Figure 39 shows the pattern sizes of an ideal phosphor screen as a function of the exposure doses of UV light. The ADC concentration for phosphor screens with $n = 2$ is 4 wt % in 100 g of PVA resin.[99]

When the phosphor screens are produced using commercial phosphor powders under the established screening procedures (specifications), one obtains the curve shown in Figure 40, instead of that in Figure 39. This curve has a constant width of the patterned screen in the high-dose range. It has been believed

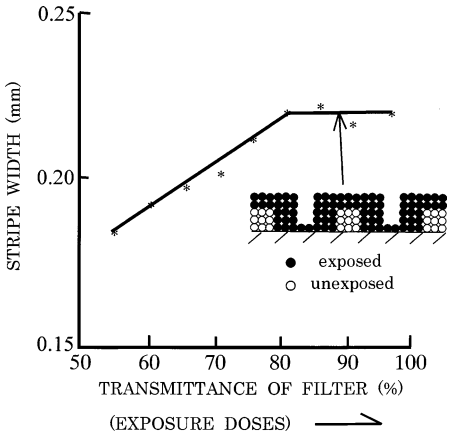

Figure 40. Pattern sizes of phosphor screens with defects as a function of the exposure doses of UV light.

by screening engineers that the constant width is a good screening condition for the CRT production. Then, they are attempting to narrow the pattern sizes by adding many surfactants available. This, however, leads to a serious problem, as described below.

The phosphor screens produced with commercial powders are usually constructed with layers of $n = 5-7$, which is calculated by using eq 14, instead of $n = 2$. This is due to the aggregation of phosphor particles in the PVA screens. The screens have many pinholes.[99] The constant pattern sizes result from the photolithography in the localized pinhole areas in the patterned screens with high ADC concentrations. The total area of patterned screens is not adhered on the faceplate, thus becoming sensitive to exposure and developing conditions. One may encounter a great deal of difficulties in achieving good reproducibility of pattern sizes. The density and size of the pinholes vary considerably with the screen size, location, and screening time. The screening conditions (specifications) for commercial phosphor powders have been empirically determined after many experiments. With poor reproducibility, a number of in-house trade secretes have been developed by screening engineers. This kind of approach is an impediment to scientific studies on the screening of phosphor powders, resulting in only a few scientific publications.[99−101]

Screening and phosphor engineers have considered that the pinholes are generated from the aggregated particles in the PVA phosphor slurry. According to them, if the surfaces are not wetted with water, the particles become aggregated in the slurry. When the particles are added in deionized water, an electric double layer is formed on the surfaces of the particles. Thus, a potential between the particle and water is formed, which is named the ξ potential. The ξ potential is reduced to a negligible value by adding a surfactant, so that the particles can disperse in the slurry. Even if the same selected surfactant is added to the PVA phosphor slurry, patterned screens obtainable change from day to day. Satisfactory patterned screens are obtained one day, but not other days. When the obtained screens are not satisfactory, other surfactants are added to the PVA slurry that has previously contained different surfactants. Eventually, the PVA phosphor slurry in practical uses contains many different kinds of surfactants to produce patterned phosphor screens.

When the PVA phosphor slurry containing many surfactants is observed by a microscope (×300 magnification), no aggregated particles will be found. However, the dried PVA phosphor screens contain many pinholes,[99] in contrast with the expectation. The observed results positively indicate that the pinholes in dried PVA phosphor screens are not directly correlated with the aggregated particles. However, screening and phosphor engineers have paid much attention to the surface potential of phosphor particles,[101] as well as the adhesion of microclusters on the surface of phosphor particles, i.e., surface treatment. Thus, the present phosphor powder and screening specifications are complicated by many additions. It should be noted that the established screening technology of phosphor powders on CRT faceplates has not been optimized scientifically, although more than 200 million CRTs were produced around the world in the year 2000. This clearly indicates that there still remains great room for further improvement of the screen luminance and image quality on the phosphor screen in CRTs.

When a PVA phosphor slurry without surfactant is prepared from the high-quality powder consisting of phosphor particles with a narrow size distribution, single shape, and clean surface, one may obtain a pinhole-free screen of $n = 2$. Bunsen−Roscow's law is applicable to the adhered pattern sizes of the screen. If the PVA phosphor slurry is prepared from this high-quality powder under established screening conditions, the resultant phosphor powder is surely rejected by screen engineers. This is because the screen is too thick for UV light to reach the bottom layer, resulting in no adhesion on the faceplate. After clarification of the screening specifications of the PVA phosphor slurry, we must design the best screenable phosphor powders, and subsequently high-resolution phosphor screens.

9. Conclusion

It has been more than 100 years since the invention of the CRT (or Braun tube). We would like to stress that the present CRTs have numerous advantages over other existing FPDs: (1) high instantaneous pixel brightness without heat, (2) high resolution of images, (3) wide viewing angle, (4) simple addressing of phosphor screens, (5) low power consumption, (6) long operation life, and (7) low production cost.[102] It is therefore predicted that CRTs will continue to be used as an important display device until the distant future, despite disadvantages such as bulky size and heavy weight. Of course, further improvement of the image quality of CRTs is necessary with a good comprehension of screening mechanisms of phosphor powders on faceplates of CRTs. One goal in the development of an ultimate CRT is that its images become comparable with printed letters on paper sheets. Then, a paperless society may be realized. This is a challenging subject for materials scientists.

10. References

(1) Leverentz, H. W. *An Introduction to Luminescence of Solids*; John Wily & Sons: New York, 1950.
(2) Kröger, F. A. *Some Aspects of the Luminescence of Solids*; Elsevier: New York, 1948.
(3) Oki, K.; Ozawa, L. *J. Soc. Inf. Display* **1995**, *3*, 51.
(4) Dekker, A. J. *Solid State Phys.* **1958**, *6*, 251.
(5) Bruning, H. *Physics and Application of Secondary Electron Emission*; Pergamon: London, 1954.
(6) Quinn, J. J. *Phys. Rev.* **1962**, *126*, 1453.
(7) Amelio, G. F. *J. Vac. Sci. Technol.* **1970**, *7*, 593.
(8) Lewis, H. W. *Phys. Rev.* **1950**, *78*, 526.
(9) Bishop, H. E. *Proc. Phys. Soc.* **1965**, *85*, 885.
(10) Bishop, H. E. *Br. J. Appl. Phys.* **1968**, *1*, 673.
(11) Murata, K.; Matsukawa, T.; Shimizu, R. *Jpn. J. Appl. Phys.* **1971**, *10*, 678.
(12) Shimizu, R.; Ikuta, T.; Murata, K. *J. Appl. Phys.* **1972**, *43*, 4233.
(13) Ehrenberg, W.; Franks, J. *Proc. Phys. Soc. (London) B* **1953**, *66*, 1057.
(14) Bowden, M. J. *J. Electrochem. Soc.* **1981**, *128*, 195C.
(15) Marton, L.; Leder, L. B. *Phys. Rev.* **1954**, *94*, 203.
(16) Watanabe, H. *J. Phys. Soc. Jpn.* **1954**, *9*, 1035.
(17) Ozawa. L.; Hersh, H. N. *Phys. Rev. Lett.* **1976**, *36*, 683.
(18) *Surface Physics of Phosphors and Semiconductors*; Scott, C. S., Reed, C. E., Eds.; Academic Press: New York, 1968.
(19) Jastrzebski, L.; Gatos, H. C.; Lagowski, J. *J. Appl. Phys.* **1977**, *48*, 1730.
(20) Gergely, G. *J. Phys. Chem. Solids* **1960**, *17*, 112.
(21) Young, J. R. *Phys. Rev.* **1955**, *99*, 1648.
(22) Prener, J. S. *J. Electrochem. Soc.* **1975**, *122*, 1516.
(23) Dowling, P. H.; Swell, J. R. *J. Electrochem. Soc.* **1953**, *100*, 22.
(24) Alves, R. V.; Buchanan, R. A.; Maple, T. G. *Appl. Phys. Lett.* **1972**, *21*, 530.
(25) Kingsley, J. D.; Prener, J. S. *J. Appl. Phys.* **1972**, *43*, 3073.
(26) Prener, J. S.; Kingsley, J. D. *J. Electrochem. Soc.* **1972**, *119*, 1254.
(27) Ignasiak, S.; Veron, H. *J. Electrochem. Soc.* **1976**, *123*, 1493.
(28) Ozawa, L.; Hersh, H. N. *J. Electrochem. Soc.* **1975**, *122*, 1222.
(29) Ozawa, L.; Hersh, H. N. *J. Electrochem. Soc.* **1974**, *121*, 894.
(30) Cole, M. W.; Cohen, M. H. *Phys. Rev. Lett.* **1969**, *23*, 1238.
(31) *X-Ray Optics and Minerals*; Descans, P., Philibert, J., Eds.; Herman: Paris, 1966.
(32) White, W. A. *Naval Res. Rep.* **1950**, 3666.
(33) Ozawa, L. *J. Electrochem. Soc.* **1981**, *128*, 140.
(34) Sommer, W. T.; Tanner, D. J. *Phys. Rev. Lett.* **1971**, *27*, 1345.
(35) Brown, T. R.; Grimes, C. C. *Phys. Rev. Lett.* **1972**, *29*, 1233.
(36) Ozawa, L.; Oki, K. *Mater. Chem. Phys.* **1999**, *60*, 274.
(37) Ozawa, L. *Cathodoluminescence*; Kodansha-VCH: Tokyo, 1990.
(38) Dietrich, H. B.; Purdy, A. E.; Murray, R. B.; Williams, R. T. *Phys. Rev. B* **1973**, *8*, 5894.
(39) Shionoya, S. In *Luminescence of Inorganic Solids*; Goldberg, P., Ed.; Academic Press: New York, 1966; p 206.
(40) Suzuki, A.; Shionoya, S. *J. Phys. Soc. Jpn.* **1971**, *31*, 1455.
(41) Hopfield, J. J.; Thomas, D. G.; Gershenzon, M. *Phys. Rev. Lett.* **1963**, *10*, 162.
(42) Thomas, D. G.; Gershenzon, M.; Trumbore, F. A. *Phys. Rev.* **1964**, *133*, A269.
(43) Dean, P. J. In *Luminescence of Inorganic Solids*; Goldberg, P., Ed.; Academic Press: New York, 1966; p 120.
(44) Shionoya, S.; Kobayashi, Y.; Koda, T. *J. Phys. Soc. Jpn.* **1965**, *20*, 2046.
(45) Klein, C. A. *J. Appl. Phys.* **1968**, *39*, 2029.
(46) Ikeda, M., unpublished data.
(47) Ozawa, L. *Application of Cathodoluminescence to Display Devices*; Kodansha: Tokyo, 1994.
(48) Dieke, G. H. *Advances in Quantum Electronics*; Columbia University Press: 1961.
(49) Johnson, L. F. *Quantum Electronics Pairs Conference*; Columbia University Press: 1963.
(50) Levine, A. K.; Palilla, F. C. *Trans. N.Y. Acad. Sci. Ser. 11* **1965**, *27*, 517.
(51) Chang, N. C. *J. Appl. Phys.* **1963**, *34*, 3500.
(52) Chang, N. C.; Gruber, J. B. *J. Chem. Phys.* **1964**, *41*, 3227.
(53) Ropp, R. C. *J. Electrochem. Soc.* **1964**, *111*, 311.
(54) Dieke, G. H.; Crosswhite, H. M. *Appl. Opt.* **1963**, *2*, 675.
(55) Margolis, J. S. *J. Chem. Phys.* **1961**, *35*, 1367.
(56) Wickersheim, K. A.; Lefever, R. A. *J. Electrochem. Soc.* **1964**, *111*, 47.
(57) Broser, I. In *Physics and Chemistry of II−VI Compounds*; Aven, M., Prener, J. S., Eds.; North-Holland: Amsterdam, 1967; p 526.
(58) Ludwig, G. W.; Kingsley J. D. *J. Electrochem. Soc.* **1970**, *117*, 348.
(59) Kingsley J. D.; Ludwig, G. W. *J. Electrochem. Soc.* **1970**, *117*, 353.
(60) Godlewski, M.; Świątek, K.; Suchocki, A.; Langer, J. M. *J. Lumin.* **1991**, *48* & *49*, 23.
(61) Balkanski, M.; Gans, F. In *Luminescence of Organic and Inorganic Materials*; Kallman, H. P., Spruch, G. M., Eds.; John Wily & Sons: New York, 1962; p 318.
(62) Garlick, G. F. J. In *Luminescence of Inorganic Solids*; Goldberg, P., Ed.; Academic Press: New York, 1966; p 685.
(63) Rothwarf, A. *J. Appl. Phys.* **1973**, *44*, 752.
(64) Yamamoto, H.; Tonomura, A. *J. Lumin.* **1976**, *12&13*, 947.
(65) Alig, R. C.; Bloom, S. *J. Electrochem. Soc.* **1977**, *124*, 1136.
(66) Lehmann, W. *J. Electrochem. Soc.* **1971**, *118*, 1164.
(67) Meyer, V. D. *J. Electrochem. Soc.* **1972**, *119*, 920.
(68) Stevels, A. L. N.; Pingault, F. *Philips Res. Rep.* **1975**, *30*, 277.
(69) Shea, L. E. *Interface* **1998**, *7*, 24.
(70) Blasse, G.; Grabmaier, B. C. *Luminescent Materials*; Springer-Verlag: Berlin, 1994.
(71) *Phosphor Handbook*; Shionoya, S., Yen, W. M., Eds.; CRC Press: Boca Raton, FL, 1998.
(72) Bril, A.; Klasens, H. A. *Philips Res. Rep.* **1952**, *7*, 401.
(73) Hase, T.; Kano, T.; Nakazawa, E.; Yamamoto, H. In *Advances in Electronics and Electron Physics*; Academic Press: New York, 1990; Vol. 79, p 311.
(74) Strehlow, W. H.; Cook, E. L. *J. Phys. Chem. Ref. Data* **1973**, *2*, 163.
(75) Itoh, M.; Inabe, Y. *Phys. Rev. B* **2003**, *68*, 035107.
(76) Tomiki, T.; Tamashiro, J.; Tanahara, Y.; Yamada, A.; Fukutani, H.; Miyahara, T.; Kato, H.; Shin, S.; Ishigame, M. *J. Phys. Soc. Jpn.* **1986**, *55*, 4543.
(77) Kingsley, J. D.; Ludwig, G. W. *J. Appl. Phys.* **1970**, *41*, 370.
(78) Kolk, E.; Dorenbos, P.; Eijk, C. W. E.; Bechtel, H.; Jüstel, T.; Nikol, H.; Ronda, C. R.; Wiechert, D. U. *J. Lumin.* **2000**, *87−89*, 1246.
(79) Alig, R. C.; Bloom, S. *Phys. Rev. Lett.* **1975**, *35*, 1522.
(80) Shionoya, S. *J. Lumin.* **1970**, *1* & *2*, 17.
(81) Stevens, M. T. *J. Electrochem. Soc.* **1978**, *125*, 288.
(82) *Standard Handbook for Electrical Engineers*, 9th ed.; Knowlton, A. E., Ed.; McGraw-Hill: New York, 1957; Sect. 16.
(83) *High Brightness Light Emitting Diodes*; Craford, M. G., Stringfellow, G. B., Eds.; Academic Press: San Diego, 1997.
(84) Nakamura, S.; T. Mukai, T.; Senoh, M. *Appl. Phys. Lett.* **1994**, *64*, 1687.
(85) King, C. N. *J. Vac. Sci. Technol. A* **1996**, *14*, 1729.
(86) Tohma, T.; Yamazaki, S.; Wzorek, D. *Inf. Display* **2001**, *11*, 20.
(87) Welker, T. *J. Lumin.* **1991**, *48* & *49*, 49.
(88) Feiedman, P. S. *Inf. Display* **1995**, *10*, 22.
(89) Tarumi, K.; Heckmeier, M.; Klasen-Memmer, M. *J. Soc. Inf. Display* **2002**, *10*, 127.
(90) Coltman, J. W.; Ebbighausen, E. G.; Altar, W. *J. Appl. Phys.* **1947**, *18*, 530.
(91) Butler, K. H.; Homer, H. H. *Illum. Eng.* **1960**, *55*, 396.
(92) Bo, H.; Takeyama, S. *Illum. Eng. Japan* **1960**, *44*, 227.
(93) Fronger, W. H. *Appl. Opt.* **1982**, *21*, 1219.
(94) Branin, P. B.; Fonger, W. H. *J. Electrochem. Soc.* **1975**, *122*, 94.
(95) Busselt, W.; Raue, R. *J. Electrochem. Soc.* **1988**, *135*, 764.
(96) Herdan, G. *Small Particle Statistics*; Elsevier: New York, 1953.
(97) Kosar, J. *Light-Sensitive System*; John Wiley & Sons: New York, 1965; Chapter 2.
(98) Sasaki, M.; Kikuchi, S. *J. Jpn. Chem. Ind.* **1967**, *70*, 2107.
(99) Ozawa, L.; Xinjia, L. *J. Soc. Inf. Display* **1998**, *6*, 285.
(100) Xurong, X.; Ozawa, L. *Chin. J. Lumin.* **1989**, *10*, 162.
(101) Oguchi, T.; Tamatani, M. *J. Electrochem. Soc.* **1986**, *133*, 841.
(102) Ozawa, L. *Mater. Chem. Phys.* **1997**, *51*, 107.

CR0203490